

Abstract

The Ozone Monitoring Instrument (OMI) onboard NASA's Aura satellite has been providing global observations of the ozone layer and key atmospheric pollutant gases, such as nitrogen dioxide (NO₂) and sulfur dioxide (SO₂), since October 2004. The data products from the same instrument provide consistent spatial and temporal coverage and permit the study of anthropogenic and natural emissions on local-to-global scales. In this paper we examine changes in SO₂ and NO₂ over some of the world's most polluted industrialized regions during the first decade of OMI observations. In terms of regional pollution changes, we see both upward and downward trends, sometimes in opposite directions for NO₂ and SO₂, for the different study areas. The trends are, for the most part, associated with economic and/or technological changes in energy use, as well as regional regulatory policies. Over the eastern US, both NO₂ and SO₂ levels decreased dramatically from 2005 to 2014, by more than 40 and 80 %, respectively, as a result of both technological improvements and stricter regulations of emissions. OMI confirmed large reductions in SO₂ over eastern Europe's largest coal power plants after installation of flue gas desulfurization devices. The North China Plain has the world's most severe SO₂ pollution, but a decreasing trend has been observed since 2011, with about a 50 % reduction in 2012–2014, due to an economic slowdown and government efforts to restrain emissions from the power and industrial sectors. In contrast, India's SO₂ and NO₂ levels from coal power plants and smelters are growing at a fast pace, increasing by more than 100 and 50 %, respectively, from 2005 to 2014. Several SO₂ hot spots observed over the Persian Gulf are probably related to oil and gas operations and indicate a possible underestimation of emissions from these sources in bottom-up emission inventories. Overall, OMI observations have proved to be very valuable in documenting rapid changes in air quality over different parts of the world during the last decade. The baseline established during the first 10 years of OMI is indispensable for the interpretation of air quality measurements from current and future satellite atmospheric composition missions.

26557

1 Introduction

Sulfur dioxide (SO₂) and nitrogen dioxide (NO₂) are reactive, short-lived atmospheric trace gases with both anthropogenic and natural sources. Major sources of NO_x (NO_x = NO + NO₂) include fossil fuel combustion, biomass burning, soil emissions (Vinken et al., 2014b) and lightning (Schumann and Huntrieser, 2007). NO₂ participates in the nitrogen cascade of air–water–soil (EPA, 2011; Galloway et al., 2013), affects atmospheric oxidation rates (Valin et al., 2013), and contributes to surface ozone production (Duncan et al., 2010; Seinfeld and Pandis, 2006). The principal sources of SO₂ are natural volcanic and anthropogenic emissions from burning sulfur-contaminated fossil fuels and the refinement of sulfide ores. Volcanic SO₂ is often injected into the atmosphere at high altitudes above the planetary boundary layer (PBL), while anthropogenic SO₂ emissions are predominantly in or slightly above the PBL. Chemical reactions in the PBL involving SO₂ and NO₂ lead to the production of aerosol oxidation products (sulfate and nitrate aerosols), and tropospheric ozone (Seinfeld and Pandis, 2006). Volatile Organic Compounds (VOCs) oxidize in the presence of NO_x and sunlight to form ozone (O₃), a major tropospheric pollutant and greenhouse gas (EPA, 2013), and the oxidation product of NO₂, nitric acid (HNO₃), reacts with ammonia (NH₃) to form ammonium nitrate aerosols. SO₂ is oxidized in gas-phase reactions with the hydroxyl radical (OH) or in aqueous-phase reactions with O₃ or hydrogen peroxide (H₂O₂) to form sulfate aerosols. The sulfate and nitrate aerosols contribute to fine particulate matter pollution with aerodynamic diameters less than 2.5 μm (PM_{2.5}), which poses serious health concerns (Lee et al., 2015; Liu et al., 2015), degrades visibility, causes acidification of water and the biosphere with adverse effects on plants and soil, and impacts weather and climate through changes in direct radiative forcing and indirectly modifying cloud formation and optical properties (IPCC Working Group 1 et al., 2013; Twohy, 2005). Consequently, SO₂, NO₂, and their oxidation products, O₃ and PM_{2.5}, are designated Criteria Pollutants (European Commission, 2015; US

26558

EPA, 2015). Space based characterization of these pollutants enables global consistent monitoring, which is independent from ground-based measuring networks.

The first space-based quantitative data on SO₂ mass in volcanic clouds after a major eruption (El Chichon, 1982) was obtained from the six-UV band NASA's Nimbus-7 Total Ozone Mapping Spectrometer (TOMS) (Krueger, 1983). The TOMS SO₂ detection sensitivity was limited by the discrete wavelengths to exceptionally strong anthropogenic emissions, such as those produced by Norilsk smelting plants in Russia or from an accidental combustion of elemental sulfur (S) at the Al-Mishraq State Sulfur Mine Plant in Iraq (Carn et al., 2004; US Department of Veterans Affairs, 2015). Greatly improved sensitivity was demonstrated through detection of SO₂ emissions from coal-fired power plants using ESA's Global Ozone Monitoring Experiment (GOME, 1995–2005) (Burrows et al., 1997; Eisinger and Burrows, 1998) and SCanning Imaging Absorption spectrometer for Atmospheric CHartography, (SCIAMACHY, 2002–2012) (Bovensmann et al., 1999) hyperspectral UV spectrometers. The first tropospheric NO₂ quantification was demonstrated using GOME and SCIAMACHY visible data (Leue et al., 2001; Martin et al., 2002; Richter and Burrows, 2002; Richter et al., 2005). These sensors needed several days to acquire a contiguous global map. The Ozone Monitoring Instrument (OMI) is the first satellite hyperspectral UV/Visible spectrometer with a push broom CCD detector and a wide, 2600-km swath (Levelt et al., 2006b), which enables daily, global contiguous mapping of ozone and other trace gases, including SO₂ and NO₂ (Levelt et al., 2006a). OMI was launched in July 2004 on NASA's Aura sun-synchronous afternoon equator crossing polar satellite (Schoeberl et al., 2006) and continues measurements through its 12th year, providing the longest data record currently available. OMI measurements are complemented with two GOME-2 instruments on EUMETSAT's MetOp-A (2006) and B (2012) operational polar satellites (Richter et al., 2011; Rix et al., 2012; Valks et al., 2011), although with lower spatial resolution and sensitivity to PBL sources (Fioletov et al., 2013). Next generation ESA's Sentinel series will provide higher spatial resolution and greater sensitivity to SO₂ and NO₂ sources (Ingmann et al., 2012; Veeffkind et al., 2012).

26559

In the PBL, both SO₂ and NO₂ have short lifetimes (< 1 day during the warm season) and are concentrated near their emission sources. This facilitates space-based detection of SO₂ and NO₂ sources and global characterization of their spatiotemporal variability (van der A et al., 2006, 2008; Burrows et al., 1999; Castellanos and Boersma, 2012; Eisinger and Burrows, 1998; Fioletov et al., 2013; de Foy et al., 2009; Hayn et al., 2009; He et al., 2012; Hilboll et al., 2013; Huang et al., 2013; Khokhar et al., 2005; Kim et al., 2009; Krotkov et al., 2008; Martin, 2008a; Martin et al., 2002; Mijling et al., 2009; Richter et al., 2005; Russell et al., 2012; Schneider and Van Der A, 2012; Theys et al., 2015; Valks et al., 2011; Zhou et al., 2009, 2012) and near-surface concentrations (Duncan et al., 2014; Lamsal et al., 2008, 2010, 2015; McLinden et al., 2014). Furthermore, over polluted regions satellite observable SO₂ and NO₂ vertically integrated number density profiles (columns) are highly correlated with underlying emissions, allowing space-based (i.e., "top-down") inference of spatial and temporal changes in emissions (van der A et al., 2008; Boersma et al., 2008, 2015; Carn et al., 2007; Ding et al., 2015; Duncan et al., 2013; Fioletov et al., 2011, 2015b; de Foy et al., 2014, 2015; Frost et al., 2006; Ghude et al., 2010, 2013; Hayn et al., 2009; He et al., 2012; Kim et al., 2009; Kononov et al., 2006, 2010; Lamsal et al., 2011; Lee et al., 2011; Li et al., 2010; Lu et al., 2013, 2015; Martin, 2008b; McLinden et al., 2012, 2014; Miyazaki et al., 2012; Napelenok et al., 2008; Reuter et al., 2014; Stavrou et al., 2008; Streets et al., 2013; Vinken et al., 2014a, b; Zhang et al., 2007), lifetime (Beirle et al., 2011; Fioletov et al., 2011, 2015b; de Foy et al., 2015; McLinden et al., 2012), physicochemical conversion (Duncan et al., 2010; Valin et al., 2013) and deposition of these species (Nowlan et al., 2014). OMI has been at the forefront of these rapid advances.

Previous OMI studies focused on specific species, emission sources and regions (van der A et al., 2008; Ahmad et al., 2007; Beirle et al., 2011; Boersma et al., 2011, 2015; Castellanos et al., 2014; Ding et al., 2015; Duncan et al., 2013; Fioletov et al., 2015b, 2011; de Foy et al., 2009, 2015; Ghude et al., 2013; Lamsal et al., 2008, 2011, 2015; Lelieveld et al., 2015; Lu et al., 2013; McLinden et al., 2014; Mebust and Cohen, 2014; Mijling and Van Der A, 2012; Mijling et al., 2009; Russell et al., 2012; Valin

26560

et al., 2013; Vinken et al., 2014a, b; Zhou et al., 2012). While NO_2 and SO_2 are both dominated by anthropogenic emissions in polluted regions, the origin of their anthropogenic sources differs, as well as the cost and efficacy of their respective emission control techniques. The often different regional trends and abundances of NO_2 and SO_2 offer valuable insights into energy infrastructures as well as pollution control policies (Li et al., 2010; McLinden et al., 2012). In this paper we examine changes in both SO_2 and NO_2 over the world's most polluted regions during the first decade of OMI observations. Section 2 briefly summarizes OMI SO_2 and NO_2 algorithms and products. Section 3 describes regional SO_2 and NO_2 changes for the world's industrial regions with large SO_2 emissions from coal burning power plants and industries (Fig. 1). For these regions the paper provides an update to the previously published trend studies and a context for a more detailed analysis of individual sources in a companion paper in this issue (Fioletov et al., 2015a).

2 OMI standard SO_2 and NO_2 products

OMI is the result of a partnership between NASA and the Dutch and Finnish meteorological institutes and space agencies (Levelt et al., 2006b) and flies on the NASA EOS-Aura satellite (Schoeberl et al., 2006). It measures sunlight backscattered from the Earth over a wide range of Ultraviolet (UV) and visible (Vis) wavelengths to derive abundances of ozone and other trace gases important for air quality and climate. The measurements of SO_2 and NO_2 are both explicit objectives of the Aura OMI mission (Levelt et al., 2006a) that are aimed at advancing our understanding of the sources and transformation processes of these pollutants and enabling the application of OMI data to inform public policy (Streets et al., 2013). Compared with other satellite UV-Vis instruments, OMI has the highest spatial resolution, least degradation and the longest record, allowing improved space-borne estimation of NO_2 and SO_2 emissions and studying their temporal behavior (Carn et al., 2007; Castellanos and Boersma, 2012;

26561

Duncan et al., 2013; Fioletov et al., 2011, 2013; de Foy et al., 2009; Lamsal et al., 2015; Lu et al., 2013; McLinden et al., 2012; Zhou et al., 2012).

Aura has a local equator crossing time of approximately 13:45 in the ascending node, and provides nearly global coverage each day. The OMI detector is a 2-dimensional Charge-Coupled Device (CCD) array. The instrument optics is designed such that the spatial dimension of the detector is oriented across the orbit track, with an 115° field of view, while the other dimension records spectral information. Three separate detectors (Dobber et al., 2006; Levelt et al., 2006b), designated UV-1, UV-2, and Vis, have spectral coverage (full performance) in the ranges of 270–310 nm (spectral resolution, full width at half maximum (FWHM), of 0.63 nm), 310–365 nm (0.45 nm), and 365–500 nm (0.63 nm), respectively. The OMI SO_2 product uses spectral measurements between 310.5 and 340 nm in the UV-2 (Li et al., 2013) and the NO_2 product uses spectral measurements between 405 and 465 nm in the Vis region (Boersma et al., 2011; Bucsel et al., 2013). The spatial dimension of both detectors is divided into 60 cross-track fields of view (FOV) corresponding to the specific binned CCD detector rows, such that rows 1 and 60 correspond to the western and eastern edges of the swath, respectively. Spectral measurements are made over 2 s exposure intervals. This results in along-track coverage of 13 km and cross-track coverage of 24 km for the near-nadir FOVs (CCD rows about 30). During each orbit, a total of about 1640 exposures are recorded on the sunlit side of the Earth. The width of the swath (2600 km) is such that 14–15 orbits per day are required to observe the entire surface of the Earth, although with increased FOV size at the swath edges. Beginning in 2007, some cross-track positions of the OMI swath were affected by FOV blockage and scattered light, also known as the “row anomaly” (KNMI, 2012). Here we use only unaffected OMI cross track positions (i.e., rows 6–23) throughout the entire mission, also excluding large FOVs at the edge of the swath.

26562

2.1 Retrieval of PBL SO₂

OMI original PBL SO₂ product employed the band residual difference (BRD) algorithm, which used only 4 discrete wavelengths (Krotkov et al., 2006). The BRD product is sensitive to PBL sources, but has a high noise level (Krotkov et al., 2008) and systematic artifacts that required empirical corrections (Fioletov et al., 2011; Lee et al., 2009). In 2014 we released a new PBL SO₂ product, which is retrieved with a new algorithm that employs a principal component analysis (PCA) technique applied to OMI radiances (Li et al., 2013). Using a clear sky Air Mass Factor (AMF) similar to the previous SO₂ product, but with the full spectral content between 310.5 and 340 nm, the PCA algorithm reduces retrieval noise by a factor of two (Li et al., 2013). Recently, the Differential Optical Absorption Spectroscopy (DOAS) SO₂ algorithm developed for the Sentinel 5 Precursor (TROPOMI) has been applied to the OMI radiances and compared with the operational PCA product (Theys et al., 2015). The two products compare well, which lends confidence in OMI SO₂ data. The estimated SO₂ noise is similar between PCA and DOAS algorithms, when using similar assumptions for AMF calculation for pollution SO₂. However, the DOAS SO₂ algorithm requires empirical corrections to remove background bias.

In this study we will use the OMI operational PCA PBL SO₂ product, which contains the vertical column density (VCD) in Dobson Units (1 DU = 2.69×10^{16} molecules cm⁻²). The product (OMSO2 v1.2.0) is publicly available from the NASA Goddard Earth Sciences (GES) Data and Information Services Center (DISC) (http://disc.sci.gsfc.nasa.gov/Aura/data-holdings/OMI/omso2_v003.shtml). The estimated 1 σ noise is ~ 0.5 DU over tropical oceanic areas (Li et al., 2013). If we assume that the noise is random and that there are about 100 cloud-free samples per year, the detection limit over low latitudes can be estimated at ~ 0.2 DU for the annual mean (signal-to-noise ratio = 2 : 1 for $\pm 1\sigma$ noise). An important advantage of the PCA algorithm is that the bias over background regions (where SO₂ columns are below the OMI detection limit) is sufficiently small (< 0.1 DU) that it requires no empirical background correction, as applied in other

26563

satellite SO₂ algorithms (e.g., Fioletov et al., 2013; Theys et al., 2015). The improved data quality, combined with the pixel averaging and oversampling techniques (e.g., de Foy et al., 2009; Beirle et al., 2011; Fioletov et al., 2011, 2013, 2015a, b; Lu et al., 2013; McLinden et al., 2012, 2014), provides greatly enhanced sensitivity to anthropogenic SO₂ sources near the surface. It has been demonstrated that US SO₂ point sources (e.g., power plants, smelters) with emissions rates as low as ~ 30 – 40 ktyr⁻¹ can be detected and analyzed using the newest OMI SO₂ product (Fioletov et al., 2015b). This limit is substantially lower than that reported (70 ktyr⁻¹) for the previous version OMI SO₂ data (Fioletov et al., 2011).

2.2 Retrieval of tropospheric NO₂

There are two algorithms used operationally to determine tropospheric NO₂ VCDs: the NASA's standard product (SP, version 2.1) and the KNMI's Dutch-OMI-NO₂ (DOMINO) algorithm (TM4NO2A, version 2, <http://www.temis.nl/airpollution/no2.html>) (Boersma et al., 2011). Both products share a common DOAS spectral fitting of laboratory-measured spectra of NO₂, H₂O, O₃, and Ring spectrum to the OMI-measured sun-normalized spectrum of backscattered radiation in the visible wavelength range of 405–465 nm to calculate NO₂ Slant Column Densities (SCDs). The estimated 1 σ noise is $\sim 10^{15}$ molecules cm⁻² or $\sim 10\%$ of the measured SCD over polluted regions (Boersma et al., 2011). The SCDs, after subtraction of the stratospheric contribution are converted to tropospheric VCDs by applying AMFs, interpolated from the Look-up-Tables (LUT) with OMI-measured input parameters such as viewing geometry, climatological surface reflectivity, cloud pressure and cloud radiance fraction, assuming a priori NO₂ vertical profile shapes. The NASA and KNMI algorithms differ in how they remove the stratospheric contribution and use different a priori tropospheric NO₂ profile shapes in the AMF calculation. DOMINO subtracts stratospheric SCD as determined in a data assimilation system, in which the measured SCDs are assimilated with the TM4 chemical transport model (Boersma et al., 2011). The SP estimates stratospheric NO₂ di-

26564

rectly from OMI data without using stratospheric chemical transport models. The AMFs are calculated with a priori NO₂ monthly mean vertical profile shapes from the NASA GMI model (Bucsela et al., 2013). Despite the differences, both algorithms produce statistically similar regional trends (see Supplement Fig. S1). Here we use the SP
5 tropospheric NO₂ VCD product version 2.1 publicly available from NASA GES DISC at http://disc.sci.gsfc.nasa.gov/Aura/data-holdings/OMI/omno2_v003.shtml. Over polluted areas the total errors in OMI tropospheric NO₂ VCDs are typically within 20% for cloud-free FOVs, as confirmed by validation studies employing in situ and remotely sensed data (Bucsela et al., 2013; Irie et al., 2012; Lamsal et al., 2015; Oetjen et al.,
10 2013).

2.3 Postprocessing of NO₂ and SO₂ data

For this study, level 2 (L2) tropospheric NO₂ and PBL SO₂ VCDs are gridded at different ground resolutions after excluding pixels possibly affected by the (1) row anomaly; (2) snow; (3) transient volcanic SO₂ clouds (Appendix A); (4) cloudy scenes (cloud
15 radiance fraction > 0.5 or > 0.2 for SO₂). The standard gridded (0.25° × 0.25°) level 3 (L3), filtered, monthly regional mean values are used in time series analyses following Lamsal et al. (2015) (Appendix B). The L3 data are publicly available from NASA GES DISC archive at <http://disc.sci.gsfc.nasa.gov/Aura/data-holdings/OMI>. We also use L2 (pixel level) data oversampled at higher resolutions (0.01° × 0.01° for NO₂ and 0.02° ×
20 0.02° for SO₂) to create global and regional maps that highlight point pollution sources. The regional maps are created directly from pre-filtered L2 data by averaging all OMI pixels within 20 km smoothing radius (30 km for SO₂) for 3–4 year time periods. Unlike previous studies (Lee et al., 2009; Fioletov et al., 2011, 2013; Lu et al., 2013; McLinden et al., 2014), no empirical background correction was applied to the PBL SO₂ data.

26565

3 Regional pollution changes and interpretation

Figure 1 shows SO₂ and NO₂ multi-year average maps at the beginning of the OMI mission (2005–2007) over the Northern Hemisphere. Regionally, population density (Lamsal et al., 2013), type of power generation and fuel used, economic activity, and
5 regulatory policies determine average levels of air pollution. The SO₂ map (Fig. 1a) shows hotspots associated with major coal-fired power plants and industrial activities, such as oil and gas refining and metal smelting. The highest SO₂ is found over industrialized and populated regions in eastern China, as the world's second largest economy relies on sulfur (S) rich coal for ~ 70 % of its energy consumption (Klimont et al., 2009;
10 Zhang and Cheng, 2009). Based on bottom-up emission inventories, SO₂ emissions from China were the world's largest, at ~ 33 Tg SO₂ in 2005 (Lu et al., 2010, 2011). High S coal-fired power plants are the major contributors to the SO₂ over the eastern US (SO₂ emissions 14.5 Tg SO₂ in 2005 (US EPA, 2014)), eastern Europe and India (~ 6.7 Tg SO₂ (Lu et al., 2011)). SO₂ is lower (undetectable) over the western US and
15 western Europe where emissions of SO₂ have been relatively small due to small share of coal-fired power plants, the low S content of coal and installation of effective flue gas desulfurization devices capable of capturing more than 95 % of SO₂ emissions (US EIA, 2010).

Large SO₂ column amounts are also observed over the Persian Gulf, due to emissions from the oil and gas industry in the region. Based on a bottom-up SO₂ emission inventory, the total SO₂ emissions from the Middle East in 2005 were ~ 6 Tg SO₂ (Smith et al., 2011b), less than those from India and the US. However, OMI-observed SO₂ columns over the Persian Gulf region are significantly larger than over these two
20 regions. This implies that real SO₂ emissions from the Middle East (particularly in the Persian Gulf) are significantly underestimated in current bottom-up emission estimates. In addition to anthropogenic SO₂, volcanic SO₂ is frequently observed over Kamchatka (Russian Federation), Japan, the South Pacific (e.g., Anatahan volcano, Mariana Islands, Mauna Loa, Hawaii), Sicily (Etna), Mexico (Popocatepetel volcano, south of
25

26566

Mexico city), Central America and Montserrat, West Indies. Although transient volcanic signals were filtered from the PBL SO₂ data (Table A1), the signals from frequently erupting (e.g., Mt. Etna, Popocatepetel) or degassing volcanos remain. Except for Mt. Etna and Mt. Popocatepetel (de Foy et al., 2009), most volcanic sources are located in remote locations and do not contribute to the SO₂ in industrial regions considered here (see OMI daily SO₂ maps for the world's volcanic regions at <http://so2.gsfc.nasa.gov>).

The average NO₂ map (Fig. 1b) is correlated with the nighttime lights map (Fig. 1c), used here as a proxy for population density and energy production (Lamsal et al., 2013). For example, the highest NO₂ levels are observed over the world's most populated and industrialized regions including eastern China, western Europe, and the eastern US, where local NO₂ "hot spots" coincide with large urban agglomerations (Schneider et al., 2015), power plants (Duncan et al., 2013; de Foy et al., 2015) and industrial complexes. NO₂ tropospheric columns over India and the Middle East are significantly less than over China, western Europe and the US. This can be explained by low NO_x emissions, especially from mobile sources, and, partly, by year-round high temperatures, leading to shorter NO₂ lifetimes (Beirle et al., 2011). For example, Indian NO_x emissions were relatively low at 5.7 Tg NO_x in 2005 (Lu and Streets, 2012), whereas those from China and the US were 16.9 Tg NO_x (Klimont et al., 2009) and 20.4 Tg NO_x (US EPA, 2014), respectively. Relatively small, but significant areal NO₂ enhancements over west African forest are caused by seasonal biomass burning NO_x emissions (Mebust and Cohen, 2014).

The differences between the spatial distributions of NO₂ and SO₂ over the large regions indicated as boxes in Fig. 1a and b are related to economic activity, fuel types, combustion technology and different regulatory policies. The most abundant source of SO₂ is Pyrite (mostly FeS₂) and organic S in lower-grade coal as well as liquid fuel, mostly contained in heterocyclic aromatic compounds in oil, which largely accounts for high SO₂ levels over the Persian Gulf from gas flaring and oil refining. Many developed countries have regulated the S content of fuels and also required catalytic exhaust gas processing, resulting in decreased mobile-source NO_x and SO₂ emissions in exhaust.

26567

Regulations are also focused on stack emissions of NO_x and SO_x (SO_x = SO₂ + SO₃) at point sources, such as power plants and smelters. This, in turn, has driven technological changes upstream to meet regulatory requirements. For example, fluidized-bed combustion technology permits burning at lower temperature, producing less NO_x, and the condensed phase chemical capture of S, producing less gaseous SO_x. Chemical Loop Combustion technology uses catalytic oxygenation to oxidize the fuel largely in the absence of N₂, again resulting in greatly reduced NO_x leaving the combustion chamber. Stack scrubbers (i.e., flue gas desulfurization devices) have been widely deployed in Europe and the US, in particular, for existing plants, to remove SO₂ and other chemicals – notably mercury – from the flue gases, in order to meet regulatory standards. However, these changes have yet to be widely implemented in developing countries.

In addition to emissions, meteorology also plays an important role in regional air pollution, particularly on relatively short time scales (days to months). For midlatitude areas discussed in this study (the eastern US, eastern China, and eastern Europe), the concentrations of SO₂ and NO₂ often exhibit large day-to-day changes. They tend to increase under the relatively stagnant conditions ahead of a cold front and decrease dramatically after the cold front brings precipitation and strong winds into the area (Li et al., 2007). On the interannual time scale, the frequency of cold front passages may be influenced by large-scale circulation patterns such as the position of the Siberian high for eastern China (Jia et al., 2015), leading to interannual changes in SO₂ and NO₂. But meteorology probably plays a lesser role in the longer-term trends that we discuss in this study. For example, given the general trend of weakening surface winds in the Northern Hemisphere (Vautard et al., 2010), one would expect both SO₂ and NO₂ to increase over time in China, with constant emissions. While OMI did initially observe growths in both SO₂ and NO₂ over China (Sect. 3.3), the different trends between the two gases after 2007 imply that different emission control measures may play a more significant role in OMI-observed trends. Similarly, the decreasing pollution levels observed over the eastern US (Sect. 3.1) and eastern Europe (Sect. 3.2) can

26568

discussed later. Overall, between 2005 and 2014 the SO_2 drop over ORV was close to 80 %, while NO_2 dropped by 40 %, the largest reductions seen in this study. The magnitude of the relative reduction in NO_2 over the I-95 corridor is similar to that over the ORV (SM: Fig. S1), suggesting similar reduction in NO_x emissions from power plants (ORV region), cities and mobile sources (I-95 region). Independent analysis of OMI NO_2 data confirmed that NO_x emissions of 35 major US urban areas decreased by $\sim 50\%$ from 2004 to 2014 (Lu et al., 2015). We also note the faster decline in NO_2 levels before 2009 because of the installation of NO_x control devices on power plants and impact of the economic recession in 2007–2009. The annual reduction rate in NO_2 has slowed since 2009 as the US economy has recovered from the recession and the implementation of further pollution controls has slowed. As result of larger SO_2 reductions, the $\text{SO}_2 / \text{NO}_2$ column ratio dropped over the ORV region from its maximal values of $\sim 4\text{--}5$ in 2005 to less than 2 in 2014 and less than 1 over I-95 corridor (SM, Fig. S2). We expect similar change in PM speciation with increasing contribution of nitrate aerosols.

Although both SO_2 and NO_2 are Criteria Pollutants, and there remain jurisdictions in the US in violation of the National Ambient Air Quality Standards (NAAQS) for these primary pollutants, just as important is their role as precursors of key secondary air pollutants such as fine particles and ozone. The greatest numbers of Americans at risk for harmful effects of air pollution are subject to exposure to these secondary pollutants (Lee et al., 2015). Ozone is the Criteria Pollutant most likely to be found in exceedance of the US National Ambient Air Quality Standards (NAAQSs), but controlling NO_x emissions is more expensive and difficult than controlling SO_2 emissions. By 2014, total US SO_2 emissions fell to about 1/6 of their 1970 peak, but NO_x emissions only fell substantially after 2000 and are now about 1/2 of their peak in 2000 (<http://www.epa.gov/ttnchie1/trends/>). Because of these NO_x reductions, photochemical smog over eastern US has improved significantly over the same time period (Castellanos et al., 2011; Hogrefe et al., 2011; Simon et al., 2015). The total deposition of oxidized N (the combination of wet and dry deposition of species such as NO_2 and

26571

NO_3^-) has improved as well (Nowlan et al., 2014) indicating that the efforts to control NO_x emissions have been successful.

3.2 Eastern Europe

Europe experienced a $\sim 80\%$ SO_2 reduction between 1990 and 2011 (EEA, 2013). Particularly, in western Europe, after significant reduction of SO_2 emissions in the 1980s–1990s, the SO_2 levels have dropped below the OMI detection limit. There are, however, detectable SO_2 sources in eastern Europe (Fig. 4). The spatial distribution of the observed SO_2 columns at the beginning of OMI mission is consistent with the spatial pattern of SO_2 concentrations derived from the surface monitoring stations for 2005 (Denby et al., 2010). Notable anthropogenic SO_2 sources include, for example, the mining and industrial districts in Donbass region in Eastern Ukraine, large coal-fired thermal power plants around the Sea of Marmara and those near Kahramanmaras in southern Turkey, as well as those near Galabovo in southeastern Bulgaria, Gorj County in southwestern Romania, Belgrade in northern Serbia, and Megalopoli in southern Greece. Most of SO_2 hot spots are due to use of local high S lignite (brown) coal for power generation and incomplete SO_2 removal from the flue gas. Figure 3 (second row) shows interannual variations in SO_2 and NO_2 columns over the Maritsa Iztok power complex in Stara Zagora, Bulgaria (see blue box in Fig. 4). Large SO_2 reductions ($\sim 50\%$) between 2011 and 2014 are consistent with the installation of desulfurization devices, while NO_2 remains approximately constant, suggesting stable electricity production. Another important source of SO_2 in the region is the Mt. Etna volcano in Sicily. OMI SO_2 retrievals indicate relatively constant SO_2 degassing from Mt. Etna during the study period, but considerable decreases in SO_2 over Megalopoli, Galabovo, and Gorj County, likely owing to more stringent SO_2 controlling measures on power plant emissions in response to mandates by the European Union. SO_2 emissions from Turkey, on the other hand, appear to have increased during the same period, particularly over Kahramanmaras, where new power plants went into service in 2006 (see <http://globalenergyobservatory.org/geoid/42972>). Increases in SO_2 over Serbia may re-

26572

flect growth in energy consumption (mainly coal) as the country's economy recovers from wars in the 1990s.

Figure 4 (bottom row) also gives the spatial distribution of OMI tropospheric NO₂ over eastern Europe, which shows enhanced columns in densely populated and industrial areas. By far the largest NO₂ level in eastern Europe was observed over Moscow, Russian Federation (Gorchakov, 2011), followed by industrial regions in south Poland, east Germany and the Czech Republic. High columns are evident over major industrial regions of Wroclaw and large cities, such as Warsaw, Athens, and Budapest. These enhancements correlate well with emissions source distribution. While road traffic is in general the most important NO_x source in Europe (EEA, 2013; Vestreng et al., 2009), in some eastern European countries the power sector is the major contributor (Zyrichidou et al., 2013). New construction and upgrades in capacity of older power plants, as well as emission control measures affect NO₂ columns (Castellanos and Boersma, 2012; Zhou et al., 2012). Several studies based on bottom-up emissions and satellite observations have reported substantial decreases in NO_x emissions and NO₂ columns in most of the western European countries due to stricter emission regulations (Castellanos and Boersma, 2012; Curier et al., 2014; EEA, 2013; Lamsal et al., 2011; Schneider et al., 2015; Vestreng et al., 2009; Zhou et al., 2012). In contrast, changes in emissions are rather small in eastern Europe (Zyrichidou et al., 2010). An increase in NO_x emissions is reported for those countries where implementation of the European Union (EU) air quality standards is less effective (AQ_Environment_EC, 2015; Vestreng et al., 2009). OMI measurements are consistent with previous studies, suggesting small or insignificant NO₂ column trends on a regional level. Changes appear to be country-specific and likely depend on the socio-economic and political situation and legislative abatement measures of the country. The EU air quality standards hold for all EU-countries (including Poland, Hungary, Bulgaria, Croatia, the Baltic States, Slovenia, Slovakia), but not for Serbia, Russia, Ukraine, Belarus, and Turkey. Some countries have asked for time extension to meet certain standards because sev-

26573

eral Member States have particular difficulties in achieving compliance with the criteria for PM and NO₂.

3.3 Eastern China

The growth of the Chinese economy over the past two decades has been mainly driven by rapid industrialization and urbanization (Huang et al., 2013) and has been accompanied by large increases in both electricity generation (mainly coal-fired power plants) and the number of vehicles on Chinese roads. As evident in Figs. 1a and 5, China has the world's highest SO₂ emissions, particularly over the high S coal-rich heavily industrial areas in Hebei, Henan and Shandong provinces in the North China Plain (NCP, blue box in Fig. 5) and Inner Mongolia (Li et al., 2010; Zhang et al., 2009), the highly populated Sichuan Basin (SB, red box in Fig. 5), the megacity clusters around Shanghai (the Yangtze River Delta, YRD – black box in Fig. 5) and Guangzhou–Hong Kong (the Pearl River Delta, PRD). Similarly, OMI retrievals also reveal much greater NO₂ over eastern China than other regions of the world (Fig. 1b), especially over NCP, YRD and PRD (Fig. 5). The NO₂ levels are relatively low over SB, but highest over YRD and PRD. The SO₂ / NO₂ column ratios were 8–10 over SB, 3–5 over NCP and less than 2 over YRD and PRD in 2005 (Fig. S4). The ratios reflect to some extent the level of modernization in the regions. The PRD and YRD have little industry but higher population and car density, therefore greater NO₂ relative to SO₂.

The overall SO₂ loading, although still at a relatively high level, has decreased over the years (Fig. 5). This is more clearly shown in the SO₂ time series in Fig. 3, which suggests that the SO₂ loading over the NCP peaked in 2007, and has since shown an overall decreasing trend despite relatively large year-to-year variations. The reduction in SO₂ during 2008–2010 may be attributed to both the economic recession and emission control measures before the 2008 Beijing Olympic Games (Li et al., 2010; Lu et al., 2011; Mijling et al., 2009; Witte et al., 2009). The temporary rebound in 2011 may reflect a resurgence in the economy due to stimulation by the government. This is followed by a dramatic ~ 50 % reduction over the three-year period during 2012–2014

26574

observations (Fig. 3). India's total annual SO₂ emissions almost doubled from 6.7 Tg in 2005 to estimated 12 Tg in 2014. In 2014, India has not only surpassed the US to be the world's second largest SO₂ emitting country, but also has reached more than 40% of the SO₂ emissions of the world's largest emitter, China.

5 3.5 Middle East

In the Middle East, abundant oil and gas deposits supply cheap and relatively clean fuels for electricity generation, water desalination, and industries. OMI detects the largest SO₂ emissions over the Persian Gulf. The sources for these emissions are apparently not included in the current global emission inventory such as the 2008 EDGAR-HTAP dataset (e.g., http://edgar.jrc.ec.europa.eu/edgar_album/v42/SO2/TOTALS/v42_SO2_2008_TOT.jpg). Based on the most recent SO₂ emission inventory, the total SO₂ emissions from the Middle East in 2005 were ~ 6 Tg (Klimont et al., 2013; Smith et al., 2011a), less than those from India and the US. However, OMI observed SO₂ columns over the Gulf region are significantly larger than those over India and US. That suggests that the real SO₂ emissions from the Middle East (particularly in the Persian Gulf) may be several times higher than current bottom-up emission estimates. This is consistent with independent OMI SO₂ retrievals (Theys et al., 2015). Inverse modeling using OMI and SCIAMACHY retrievals also suggests an underestimate of SO₂ emissions from the Persian Gulf (Lee et al., 2011).

In-situ measurements of SO₂ and other pollutants are rarely reported for the region, but available data generally indicate significant SO₂ loading over the Persian Gulf. For example, an aircraft campaign conducted north of the United Arab Emirates during winter 2001 measured SO₂ concentrations of up to 40 ppb (see https://www.rap.ucar.edu/asr2002/i-precip_physics/precip_physics.htm), greater than what has been previously observed over eastern China (Dickerson et al., 2007; He et al., 2012). The largest hotspot observed by the aircraft, near Zirku Island, also appears to be co-located with a hotspot in OMI retrievals. In another study, passive sampling of SO₂ at various locations on Khark Island near the north end of the Gulf during 2003–

26577

2004 reported that the SO₂ loading was above the air quality standard (sometimes by several-fold) most of the time (Pourzamani et al., 2012). These high SO₂ columns over the Persian Gulf are likely the result of gas flaring activities from offshore oil and natural gas facilities, although shipping emissions and other sources may also contribute to them. Gas flaring is used on offshore oil rigs to dispose of gases such as hydrogen sulfide (H₂S) for safety, operational, and economic reasons and can have significant impacts on the local and regional environment in the Middle East.

Middle East cities also show SO₂ emissions due to both mobile and stationary sources. Oil-burning boilers may constitute another important source of SO₂ in cities or population centers, as implied by the relatively high sulfate (~ 10 µg m⁻³) that is closely associated with oil combustion tracers (e.g., vanadium), according to an aerosol source apportionment study for Kuwait City (Alolayan et al., 2013). The S content in gasoline and diesel is much higher in this region as compared with others such as Europe, which enforces stricter emission control measures (see <http://www.unep.org/transport/pcf/PDF/JordanWrkshp-MiddleEastFuelQuality.pdf>). Some of the largest point SO₂ sources in the region coincide with smelters or oil refineries, such as the Sarcheshmeh Copper Complex in Kerman Province, Iran, which is the largest copper smelter in the Middle East. Figure 3 (bottom row) show interannual variations in observed SO₂ and NO₂ columns over Persian Gulf (blue box in Fig. 7). Since 2010 SO₂ columns have steadily dropped by ~ 20%, but increased again in 2014 to 2005 levels (but still less than 2010 levels). A recent study (Lelieveld et al., 2015) reported that OMI SO₂ over Persian Gulf increased between 2005 and 2010, and then decreased between 2010 and 2014. Their results are based on retrievals using a different algorithm, but are qualitatively consistent with this study.

OMI retrieved regional NO₂ levels over Middle East are much smaller than over China (Fig. 6) and the US (Fig. 2). This may also be the results of the short lifetime of NO₂ in this hot and photochemically active region (Beirle et al., 2011). NO_x emissions in the region are associated with power generation and mobile sources. Local NO₂ enhancements coincide with heavily populated cities that have high car densities, such

26578

as Jerusalem (Israel) and Cairo (Egypt) (Boersma et al., 2009), Tehran (Iran), Kuwait City (Kuwait), Dubai (UAE), Riyadh and Jeddah (Saudi Arabia). In terms of regional trend over the Persian Gulf (blue box in Fig. 7), NO₂ columns increased by ~20% between 2005 and 2008, but remained approximately constant afterwards (Fig. 3). For major metropolitan areas in the region, Lelieveld et al. (2015) focused on the reversal of OMI NO₂ trends due to recent air quality regulations and domestic and international conflicts in the region. Their results are, for the most part, qualitatively consistent with Fig. 7. For example, their reported decrease of NO₂ over Damascus, Syria since 2011 (due to civil war) and increase over Baghdad, Iraq since 2007 are also visible in Fig. 7.

10 4 Conclusions

The first decade of OMI observations (2005–2014) have yielded profound insights into the spatial distribution and temporal trends in SO₂ and NO₂ around the world. For regions with detailed bottom-up emissions estimates or continuous emissions monitoring, OMI shows generally good agreement with these independent data sources. OMI-derived trends also agree well with those from available in situ measurements and deposition data. This adds confidence to the use of OMI to track locations, changes, and transport patterns of SO₂ and NO₂ over areas of the planet lacking local observations. In many regions pollution levels have changed dramatically reflecting underlying changes in SO₂ and NO_x emissions (Fig. 8): (1) over the eastern US, both NO₂ and SO₂ levels decreased dramatically from 2005 to 2014. SO₂ concentrations over the Ohio River Valley and western Pennsylvania fell by 80%, consistent with the National Emission Inventory (NEI), which reports a decrease of about 66% for total US emissions. NO₂ concentrations over the eastern US fell by more than 40%, also consistent with the NEI trend for emissions from the entire country. The Clean Air Act Amendments and regulations such as CAIR mandated these emissions reductions, and OMI confirmed their efficacy. (2) Over eastern Europe, OMI observed substantial (more than 50%) SO₂ decreases in the vicinity of the largest coal-fired power plants, where FGD

26579

was installed during the study period. Over some areas including Turkey and Serbia, local SO₂ increased, perhaps because of increased industrial activity. NO₂ levels in the vicinity of the largest eastern European power plants in Bulgaria remain constant. (3) Over China, highest SO₂ and NO₂ levels are observed over the North China Plain, with the highest concentrations in the world. SO₂ peaked in 2007, with a secondary peak in 2011, but by 2014 SO₂ has fallen to half of the levels seen at the beginning of the OMI record in 2005. Total Chinese electricity production and coal combustion have increased during the same period, and the observed decrease likely has resulted from centralization of industry and power production and the implementation of pollution control devices. NO₂ concentrations peaked in 2011, but by 2014 have returned to 2005 levels. (4) Over India, despite relatively low levels as compared with China, both SO₂ and NO₂ have increased, particularly over the northeast where a large number of newly built coal power plants have doubled SO₂ while increasing NO₂ by ~50%. This is the fastest increase in pollution concentrations observed by OMI. In 2014 India has surpassed the US to become the world's second largest SO₂ emitting country. (5) Over the Middle East, OMI detected several SO₂ hot spots with a broad maximum over the Persian Gulf region. These hotspots are probably related to oil and gas operations but are mostly absent in bottom-up emission inventories, such as EDGAR. High concentrations of NO₂ are observed over major cities but less so over oil and gas operations. SO₂ shows no discernable trend over the Gulf while NO₂ rose from 2005 to 2008 and has since remained largely unchanged.

In summary, this study demonstrates that satellite remote sensing from advanced instruments such as OMI can provide long-term, nearly continuous global monitoring of SO₂ and NO₂. Where in situ concentration measurements, emission inventories, and deposition monitoring are available, OMI provides complementary measurements to supplement and verify those other data sources. It can also find unreported or underreported major emissions such as over the Persian Gulf. OMI SO₂ and NO₂ data can also help to further our understanding of the production and impact of secondary pollutants such as tropospheric ozone and particulate matter.

26580

Space-based monitoring plays an increasingly important role in the science of tropospheric chemistry and air quality applications to help mitigate anthropogenic and natural impacts on climate, sensitive ecosystems, and human health. It is essential to continue and maintain overlapping long-term satellite data records. The baseline established during the first 10 years of OMI is invaluable for the interpretation of measurements from future satellite atmospheric chemistry missions. The OMI NO₂ and SO₂ data sets used in this study will be continued by the TROPOspheric Monitoring Instrument (TROPOMI) (Veefkind et al., 2012), which is planned for launch on ESA's Sentinel 5 Precursor satellite in 2016. TROPOMI will have a significantly higher signal-to-noise and spatial resolution (7 km × 7 km at nadir) than OMI (13 km × 24 km at nadir); both features are very important for monitoring point pollution sources and trends. TROPOMI is part of the European Sentinel series that will continue the global pollution data record for another 20 years (Ingmann et al., 2012). The space-based capabilities for air quality applications will be further enhanced by the addition of high-ground resolution (at 4 km by 4 km at nadir) hourly observations from the three geostationary satellites over North America (TEMPO, <http://tempo.si.edu>), over Europe (Sentinel 4 UVN (Ingmann et al., 2012)) and East Asia (GEMS). This constellation will allow for unprecedented observations of the key pollutants in the atmosphere.

Appendix A: Filtering transient volcanic clouds

Days affected by transient volcanic SO₂ signals were excluded as follows. Every day the region-wide 99.9-percentile of SO₂ VCDs was computed. If it was found to exceed a threshold value (Table A1) then all data from that day were excluded. This was found to perform better than a simple maximum SO₂ or NO₂ column cut-off as it tended to remove volcanic signals that, while elevated, would not exceed the maximum. A disadvantage of this method is that, while the volcanic contamination would generally only impact a small portion of the region, all data from that day were removed. The SO₂ threshold employed varied from 5 to 10 DU (Table A1) and was chosen by examining

26581

the 99.9-percentile time series during known periods of minimal volcanic activity. Different regions were found to be affected differently, a result of their proximity to significant eruptions. For regions that span the northern mid-latitudes such as US, Europe, and China, many of the days occurred in 2008 and 2009 and can be attributed to the eruptions of Kasatochi (Aleutian Islands, Alaska, August 2008, 52° N) and Sarychev (Kuril Islands, eastern Russia, June 2009, 48° N). By contrast, the Nabro eruption (northern Africa, June 2011, 13.37° N) removed the most days over India and Africa whereas the Middle East appeared to be largely unaffected by volcanic emissions.

Appendix B: Timeseries analysis

We use standard Level 3 monthly regional mean SO₂ and NO₂ columns and a regression model discussed in Lamsal et al. (2015) to compare inter-annual timeseries for different regions. The time series of monthly average values (Ω) are assumed to be comprised of three additive subcomponents: a seasonal component (α), a linear trend component (β), and residues or noise (R) component:

$$\Omega(t) = \alpha(t) + \beta t + R(t) \quad (\text{B1})$$

where, t represents time (month). The time dependent seasonal regression coefficient (α) is given by a constant plus intra-annual sine and cosine harmonic series (Randel and Cobb, 1994):

$$\alpha(t) = c_0 + \sum_{j=1}^3 \left(c_{1j} \sin\left(\frac{2\pi jt}{12}\right) + c_{2j} \cos\left(\frac{2\pi jt}{12}\right) \right), \quad (\text{B2})$$

where c_0 , c_{1j} , and c_{2j} are constant coefficients. The major portion of the annual cycle is explained by the seasonal variation of the NO_x and SO₂ lifetime. Other factors, such as monthly variation in source strength, could also affect the annual variation of NO₂ and SO₂ columns, but these contributions especially for NO₂ to the seasonal cycle are

26582

- tropospheric NO₂ retrieval algorithm for nadir-viewing satellite instruments: applications to OMI, *Atmos. Meas. Tech.*, 6, 2607–2626, doi:10.5194/amt-6-2607-2013, 2013.
- Burrows, J. P., Buchwitz, M., Rozanov, V., Weber, M., Richter, A., Ladstätter-Weißmayer, A., and Eisinger, M.: The Global Ozone Monitoring Experiment (GOME): Mission, Instrument
 5 Concept, and First Scientific Results, *Eur. Sp. Agency, Special Publ. ESA SP, 414 PART 2, 585–590*, doi:10.1175/1520-0469(1999)056<0151:TGOMEG>2.0.CO;2, 1997.
- Burrows, J. P., Weber, M., Buchwitz, M., Rozanov, V., and Ladst, A.: The Global Ozone Monitoring Experiment (GOME): mission concept and first scientific results, *J. Atmos. Sci.*, 56, 151–175, 1999.
- 10 CAAA: EPA History: Clean Air Act Amendments of 1990, available at: <http://www2.epa.gov/aboutepa/epa-history-clean-air-act-amendments-1990> (last access: 9 August 2015), 1990.
- CAIR: Programs, Clean Air Markets, US Environmental Protection Agency, available at: <http://www.epa.gov/airmarkets/programs/index.html> (last access: 9 August 2015), 2009.
- Carn, S. A., Krueger, A. J., Krotkov, N. A., and Gray, M. A.: Fire at Iraqi sulfur plant emits SO₂ clouds detected by Earth Probe TOMS, *Geophys. Res. Lett.*, 31, 2–5,
 15 doi:10.1029/2004GL020719, 2004.
- Carn, S. A., Krueger, A. J., Krotkov, N. A., Yang, K., and Levelt, P. F.: Sulfur dioxide emissions from Peruvian copper smelters detected by the Ozone Monitoring Instrument, *Geophys. Res. Lett.*, 34, L09801, doi:10.1029/2006GL029020, 2007.
- 20 Castellanos, P. and Boersma, K. F.: Reductions in nitrogen oxides over Europe driven by environmental policy and economic recession, *Sci. Rep.*, 2, 265, doi:10.1038/srep00265, 2012.
- Castellanos, P., Marufu, L. T., Doddridge, B. G., Taubman, B. F., Schwab, J. J., Hains, J. C., Ehrman, S. H., and Dickerson, R. R.: Ozone, oxides of nitrogen, and carbon monoxide during pollution events over the eastern United States: an evaluation of emissions and vertical
 25 mixing, *J. Geophys. Res.*, 116, D16307, doi:10.1029/2010JD014540, 2011.
- Castellanos, P., Boersma, K. F., and van der Werf, G. R.: Satellite observations indicate substantial spatiotemporal variability in biomass burning NO_x emission factors for South America, *Atmos. Chem. Phys.*, 14, 3929–3943, doi:10.5194/acp-14-3929-2014, 2014.
- Curier, R. L., Kranenburg, R., Segers, A. J. S., Timmermans, R. M. A., and Schaap, M.: Synergistic use of OMI NO₂ tropospheric columns and LOTOS–EUROS to evaluate the NO_x emission trends across Europe, *Remote Sens. Environ.*, 149, 58–69,
 30 doi:10.1016/j.rse.2014.03.032, 2014.

26585

- Denby, B., Sundvor, I., Cassiani, M., de Smet, P., de Leeuw, F., and Horálek, J.: Spatial mapping of ozone and SO₂ trends in Europe, *Sci. Total Environ.*, 408, 4795–4806, doi:10.1016/j.scitotenv.2010.06.021, 2010.
- Dickerson, R. R., Li, C., Li, Z., Marufu, L. T., Stehr, J. W., McClure, B., Krotkov, N., Chen, H.,
 5 Wang, P., Xia, X., Ban, X., Gong, F., Yuan, J., and Yang, J.: Aircraft observations of dust and pollutants over northeast China: insight into the meteorological mechanisms of transport, *J. Geophys. Res.-Atmos.*, 112, 1–13, doi:10.1029/2007JD008999, 2007.
- Ding, J., van der A, R. J., Mijling, B., Levelt, P. F., and Hao, N.: NO_x emission estimates during the 2014 Youth Olympic Games in Nanjing, *Atmos. Chem. Phys.*, 15, 9399–9412,
 10 doi:10.5194/acp-15-9399-2015, 2015.
- Dobber, M. R., Dirksen, R. J., Levelt, P. F., Van Den Oord, G. H. J., Voors, R. H. M., Kleipool, Q., Jaross, G., Kowalewski, M., Hilsenrath, E., Leppelmeier, G. W., de Vries, J. D. V. J., Dierssen, W., and Rozemeijer, N. C.: Ozone monitoring instrument calibration, *IEEE T. Geosci. Remote*, 44, 1209–1238, doi:10.1109/TGRS.2006.869987, 2006.
- 15 Duncan, B. N., Yoshida, Y., Olson, J. R., Sillman, S., Martin, R. V., Lamsal, L., Hu, Y., Pickering, K. E., Retscher, C., Allen, D. J., and Crawford, J. H.: Application of OMI observations to a space-based indicator of NO_x and VOC controls on surface ozone formation, *Atmos. Environ.*, 44, 2213–2223, doi:10.1016/j.atmosenv.2010.03.010, 2010.
- Duncan, B. N., Yoshida, Y., de Foy, B., Lamsal, L. N., Streets, D. G., Lu, Z., Pickering, K. E., and
 20 Krotkov, N. A.: The observed response of Ozone Monitoring Instrument (OMI) NO₂ columns to NO_x emission controls on power plants in the United States: 2005–2011, *Atmos. Environ.*, 81, 102–111, doi:10.1016/j.atmosenv.2013.08.068, 2013.
- Duncan, B. N., Prados, A. I., Lamsal, L. N., Liu, Y., Streets, D. G., Gupta, P., Hilsenrath, E., Kahn, R. A., Nielsen, J. E., Beyersdorf, A. J., Burton, S. P., Fiore, A. M., Fishman, J., Henze, D. K., Hostetler, C. A., Krotkov, N. A., Lee, P., Lin, M., Pawson, S., Pfister, G., Pickering, K. E.,
 25 Pierce, R. B., Yoshida, Y., and Ziemba, L. D.: Satellite data of atmospheric pollution for US air quality applications: examples of applications, summary of data end-user resources, answers to FAQs, and common mistakes to avoid, *Atmos. Environ.*, 94, 647–662, doi:10.1016/j.atmosenv.2014.05.061, 2014.
- 30 EEA: European Union Emission Inventory Report 1990–2011 Under the UNECE Convention on Long-range Transboundary Air Pollution (LRTAP), European Environment Agency (EEA), Technical report No 10/2013, doi:10.2800/44480, 2013.

26586

- Eisinger, M. and Burrows, J. P.: Tropospheric sulfur dioxide observed by the ERS-2 GOME instrument, *Geophys. Res. Lett.*, 25, 4177–4180, doi:10.1029/1998GL900128, 1998.
- EPA: Reactive Nitrogen in the United States: An Analysis of Inputs, Flows, Consequences, and Management Options, Washington, DC, available at: [http://yosemite.epa.gov/sab/sabproduct.nsf/WebBOARD/INCFullReport/\\$File/FinalINCRReport_8_19_11\(withoutsignatures\).pdf](http://yosemite.epa.gov/sab/sabproduct.nsf/WebBOARD/INCFullReport/$File/FinalINCRReport_8_19_11(withoutsignatures).pdf) (last access: 12 July 2015), 2011.
- EPA: Integrated Science Assessment of Ozone and Related Photochemical Oxidants, available at: <http://cfpub.epa.gov/ncea/isa/recordisplay.cfm?deid=247492#Download> (last access: 12 July 2015), 2013.
- European Commission: Air Quality Standards – Environment – European Commission, available at: <http://ec.europa.eu/environment/air/quality/standards.htm> (last access: 5 August 2015), 2015.
- Fioletov, V. E., McLinden, C. A., Krotkov, N., Moran, M. D., and Yang, K.: Estimation of SO₂ emissions using OMI retrievals, *Geophys. Res. Lett.*, 38, L21811, doi:10.1029/2011GL049402, 2011.
- Fioletov, V. E., McLinden, C. A., Krotkov, N., Yang, K., Loyola, D. G., Valks, P., Theys, N., Van Roozendaal, M., Nowlan, C. R., Chance, K., Liu, X., Lee, C., and Martin, R. V.: Application of OMI, SCIAMACHY, and GOME-2 satellite SO₂ retrievals for detection of large emission sources, *J. Geophys. Res.-Atmos.*, 118, 11399–11418, doi:10.1002/jgrd.50826, 2013.
- Fioletov, V. E., McLinden, C., Krotkov, N. A., and Li, C.: A global catalogue of SO₂ sources and emissions derived from Ozone Monitoring Instrument, *Atmos. Chem. Phys. Discuss.*, in preparation, 2015a.
- Fioletov, V. E., McLinden, C. A., Krotkov, N., and Li, C.: Lifetimes and emissions of SO₂ from point sources estimated from OMI, *Geophys. Res. Lett.*, 42, 1969–1976, doi:10.1002/2015GL063148, 2015b.
- de Foy, B., Krotkov, N. A., Bei, N., Herndon, S. C., Huey, L. G., Martínez, A.-P., Ruiz-Suárez, L. G., Wood, E. C., Zavala, M., and Molina, L. T.: Hit from both sides: tracking industrial and volcanic plumes in Mexico City with surface measurements and OMI SO₂ retrievals during the MILAGRO field campaign, *Atmos. Chem. Phys.*, 9, 9599–9617, doi:10.5194/acp-9-9599-2009, 2009.
- De Foy, B., Wilkins, J. L., Lu, Z., Streets, D. G., and Duncan, B. N.: Model evaluation of methods for estimating surface emissions and chemical lifetimes from satellite data, *Atmos. Environ.*, 98, 66–77, doi:10.1016/j.atmosenv.2014.08.051, 2014.

26587

- De Foy, B., Lu, Z., Streets, D. G., Lamsal, L. N., and Duncan, B. N.: Estimates of power plant NO_x emissions and lifetimes from OMI NO₂ satellite retrievals, *Atmos. Environ.*, 116, 1–11, doi:10.1016/j.atmosenv.2015.05.056, 2015.
- Frost, G. J., McKeen, S. A., Trainer, M., Ryerson, T. B., Neuman, J. A., Roberts, J. M., Swanson, A., Holloway, J. S., Sueper, D. T., Fortin, T., Parrish, D. D., Fehsenfeld, F. C., Flocke, F., Peckham, S. E., Grell, G. A., Kowal, D., Cartwright, J., Auerbach, N., and Habermann, T.: Effects of changing power plant NO_x emissions on ozone in the eastern United States: proof of concept, *J. Geophys. Res.*, 111, D12306, doi:10.1029/2005JD006354, 2006.
- Galloway, J. N., Leach, A. M., Bleeker, A., and Erisman, J. W.: A chronology of human understanding of the nitrogen cycle, *Philos. T. R. Soc. Lond.*, 368, doi:10.1098/rstb.2013.0120, 2013.
- Ghude, S. D., Lal, D. M., Beig, G., Van Der A, R., and Sable, D.: Rain-induced soil NO_x emission from India during the onset of the summer monsoon: a satellite perspective, *J. Geophys. Res.-Atmos.*, 115, D16304, doi:10.1029/2009JD013367, 2010.
- Ghude, S. D., Kulkarni, P. S., Kulkarni, S. H., Fadnavis, S., and Van Der A, R. J.: Temporal variation of urban NO_x concentration in India during the past decade as observed from space, *Int. J. Remote Sens.*, 32, 849–861, doi:10.1080/01431161.2010.517797, 2011.
- Ghude, S. D., Pfister, G. G., Jena, C., Van Der A, R. J., Emmons, L. K., and Kumar, R.: Satellite constraints of nitrogen oxide (NO_x) emissions from India based on OMI observations and WRF-Chem simulations, *Geophys. Res. Lett.*, 40, 423–428, doi:10.1029/2012GL053926, 2013.
- Gorchakov, G., Semoutnikova, E., Karpov, A., and Lezina, E.: Air Pollution in Moscow Megacity, Chapter 11, in: *Advanced Topics in Environmental Health and Air Pollution Case Studies*, edited by: Moldoveanu, A. M., InTech., 2011.
- Guay, J.: China's thirst for coal is drying up, available at: http://www.huffingtonpost.com/justin-guay/chinas-thirst-for-coal-is_b_5358194.html (last access: 26 August 2015), 2015.
- Hand, J. L., Schichtel, B. A., Malm, W. C., and Pitchford, M. L.: Particulate sulfate ion concentration and SO₂ emission trends in the United States from the early 1990s through 2010, *Atmos. Chem. Phys.*, 12, 10353–10365, doi:10.5194/acp-12-10353-2012, 2012.
- Hayn, M., Beirle, S., Hamprecht, F. A., Platt, U., Menze, B. H., and Wagner, T.: Analysing spatio-temporal patterns of the global NO₂-distribution retrieved from GOME satellite observations using a generalized additive model, *Atmos. Chem. Phys.*, 9, 6459–6477, doi:10.5194/acp-9-6459-2009, 2009.

26588

- He, H., Li, C., Loughner, C. P., Li, Z., Krotkov, N. A., Yang, K., Wang, L., Zheng, Y., Bao, X., Zhao, G., and Dickerson, R. R.: SO₂ over central China?: measurements, numerical simulations and the tropospheric sulfur budget, *J. Geophys. Res.-Atmos.*, 117, 1–15, doi:10.1029/2011JD016473, 2012.
- 5 Hilboll, A., Richter, A., and Burrows, J. P.: Long-term changes of tropospheric NO₂ over megacities derived from multiple satellite instruments, *Atmos. Chem. Phys.*, 13, 4145–4169, doi:10.5194/acp-13-4145-2013, 2013.
- Hogrefe, C., Hao, W., Zalewsky, E. E., Ku, J.-Y., Lynn, B., Rosenzweig, C., Schultz, M. G., Rast, S., Newchurch, M. J., Wang, L., Kinney, P. L., and Sistla, G.: An analysis of long-term regional-scale ozone simulations over the Northeastern United States: variability and trends, *Atmos. Chem. Phys.*, 11, 567–582, doi:10.5194/acp-11-567-2011, 2011.
- 10 Huang, J., Zhou, C., Lee, X., Bao, Y., Zhao, X., Fung, J., Richter, A., Liu, X., and Zheng, Y.: The effects of rapid urbanization on the levels in tropospheric nitrogen dioxide and ozone over East China, *Atmos. Environ.*, 77, 558–567, doi:10.1016/j.atmosenv.2013.05.030, 2013.
- 15 Ingmann, P., Veihelmann, B., Langen, J., Lamarre, D., Stark, H., and Courrèges-Lacoste, G. B.: Requirements for the GMES Atmosphere Service and ESA's implementation concept: Sentinels-4/-5 and -5p, *Remote Sens. Environ.*, 120, 58–69, doi:10.1016/j.rse.2012.01.023, 2012.
- IPCC Working Group 1, Stocker, T. F., Qin, D., Plattner, G.-K., Tignor, M., Allen, S. K., Boschung, J., Nauels, A., Xia, Y., Bex, V., and Midgley, P. M.: IPCC, 2013: Climate Change 2013: The Physical Science Basis. Contribution of Working Group I to the Fifth Assessment Report of the Intergovernmental Panel on Climate Change, IPCC, AR5, 1535, 2013.
- 20 Irie, H., Boersma, K. F., Kanaya, Y., Takashima, H., Pan, X., and Wang, Z. F.: Quantitative bias estimates for tropospheric NO₂ columns retrieved from SCIAMACHY, OMI, and GOME-2 using a common standard for East Asia, *Atmos. Meas. Tech.*, 5, 2403–2411, doi:10.5194/amt-5-2403-2012, 2012.
- Jia, B., Wang, Y., Yao, Y., and Xie, Y.: A new indicator on the impact of large-scale circulation on wintertime particulate matter pollution over China, *Atmos. Chem. Phys. Discuss.*, 15, 19275–19304, doi:10.5194/acpd-15-19275-2015, 2015.
- 30 Khokhar, M. F., Frankenberg, C., Van Roozendaal, M., Beirle, S., Köhl, S., Richter, A., Platt, U., and Wagner, T.: Satellite observations of atmospheric SO₂ from volcanic eruptions during the time-period of 1996–2002, *Adv. Space Res.*, 36, 879–887, 2005.

26589

- Kim, S. W., Heckel, A., Frost, G. J., Richter, A., Gleason, J., Burrows, J. P., McKeen, S., Hsie, E. Y., Granier, C., and Trainer, M.: NO₂ columns in the western United States observed from space and simulated by a regional chemistry model and their implications for NO_x emissions, *J. Geophys. Res.-Atmos.*, 114, D11301, doi:10.1029/2008JD011343, 2009.
- 5 Klimont, Z., Cofala, J., Xing, J., Wei, W., Zhang, C., Wang, S., Kejun, J., Bhandari, P., Mathur, R., Purohit, P., Rafaj, P., Chambers, A., Amann, M., and Hao, J.: Projections of SO₂, NO_x and carbonaceous aerosols emissions in Asia, *Tellus B*, 61, 602–617, doi:10.3402/tellusb.v61i4.16858, 2009.
- Klimont, Z., Smith, S. J., and Cofala, J.: The last decade of global anthropogenic sulfur dioxide: 2000–2011 emissions, *Environ. Res. Lett.*, 8, 014003, doi:10.1088/1748-9326/8/1/014003, 2013.
- KNMI: Background information about the Row Anomaly in OMI, available at: <http://www.knmi.nl/omi/research/product/rowanomaly-background.php> (last access: 5 August 2015), 2012.
- Kononov, I. B., Beekmann, M., Richter, A., and Burrows, J. P.: Inverse modelling of the spatial distribution of NO_x emissions on a continental scale using satellite data, *Atmos. Chem. Phys.*, 6, 1747–1770, doi:10.5194/acp-6-1747-2006, 2006.
- 15 Kononov, I. B., Beekmann, M., Richter, A., Burrows, J. P., and Hilboll, A.: Multi-annual changes of NO_x emissions in megacity regions: nonlinear trend analysis of satellite measurement based estimates, *Atmos. Chem. Phys.*, 10, 8481–8498, doi:10.5194/acp-10-8481-2010, 2010.
- 20 Krotkov, N. A., Cam, S. A., Krueger, A. J., Bhartia, P. K., and Yang, K.: Band residual difference algorithm for retrieval of SO₂ from the aura Ozone Monitoring Instrument (OMI), *IEEE T. Geosci. Remote*, 44, 1259–1266, doi:10.1109/TGRS.2005.861932, 2006.
- Krotkov, N. A., McClure, B., Dickerson, R. R., Carn, S. A., Li, C., Bhartia, P. K., Yang, K., Krueger, A. J., Li, Z., Levelt, P. F., Chen, H., Wang, P., and Lu, D.: Validation of SO₂ retrievals from the Ozone Monitoring Instrument over NE China, *J. Geophys. Res.-Atmos.*, 113, D16S40, doi:10.1029/2007JD008818, 2008.
- Krueger, A. J.: Sighting of el chichon sulfur dioxide clouds with the Nimbus 7 Total Ozone Mapping Spectrometer, *Science*, 220, 1377–1379, doi:10.1126/science.220.4604.1377, 1983.
- 30 Lamsal, L. N., Martin, R. V., van Donkelaar, A., Steinbacher, M., Celarier, E. A., Bucsela, E., Dunlea, E. J., and Pinto, J. P.: Ground-level nitrogen dioxide concentrations inferred from the satellite-borne Ozone Monitoring Instrument, *J. Geophys. Res.-Atmos.*, 113, D16308, doi:10.1029/2007JD009235, 2008.

26590

- Lamsal, L. N., Martin, R. V., Van Donkelaar, A., Celarier, E. A., Bucsela, E. J., Boersma, K. F., Dirksen, R., Luo, C., and Wang, Y.: Indirect validation of tropospheric nitrogen dioxide retrieved from the OMI satellite instrument: insight into the seasonal variation of nitrogen oxides at northern midlatitudes, *J. Geophys. Res.-Atmos.*, 115, D05302, doi:10.1029/2009JD013351, 2010.
- Lamsal, L. N., Martin, R. V., Padmanabhan, A., van Donkelaar, A., Zhang, Q., Sioris, C. E., Chance, K., Kurosu, T. P., and Newchurch, M. J.: Application of satellite observations for timely updates to global anthropogenic NO_x emission inventories, *Geophys. Res. Lett.*, 38, L05810, doi:10.1029/2010GL046476, 2011.
- Lamsal, L. N., Martin, R. V., Parrish, D. D., and Krotkov, N. A.: Scaling relationship for NO₂ pollution and urban population size: a satellite perspective, *Environ. Sci. Technol.*, 47, 7855–7861, doi:10.1021/es400744g, 2013.
- Lamsal, L. N., Duncan, B. N., Yoshida, Y., Krotkov, N. A., Pickering, K. E., Streets, D. G., and Lu, Z.: US NO₂ trends (2005–2013): EPA Air Quality System (AQS) data versus improved observations from the Ozone Monitoring Instrument (OMI), *Atmos. Environ.*, 110, 130–143, doi:10.1016/j.atmosenv.2015.03.055, 2015.
- Lee, C., Martin, R. V., Van Donkelaar, A., O’Byrne, G., Krotkov, N., Richter, A., Huey, L. G., and Holloway, J. S.: Retrieval of vertical columns of sulfur dioxide from SCIAMACHY and OMI: Air mass factor algorithm development, validation, and error analysis, *J. Geophys. Res.-Atmos.*, 114, D22303, doi:10.1029/2009JD012123, 2009.
- Lee, C., Martin, R. V., Van Donkelaar, A., Lee, H., Dickerson, R. R., Hains, J. C., Krotkov, N., Richter, A., Vinnikov, K., and Schwab, J. J.: SO₂ emissions and lifetimes: estimates from inverse modeling using in situ and global, space-based (SCIAMACHY and OMI) observations, *J. Geophys. Res.-Atmos.*, 116, D06304, doi:10.1029/2010JD014758, 2011.
- Lee, C. J., Martin, R. V., Henze, D. K., Brauer, M., Cohen, A., and Van Donkelaar, A.: Response of global particulate-matter-related mortality to changes in local precursor emissions, *Environ. Sci. Technol.*, 49, 4335–4344, doi:10.1021/acs.est.5b00873, 2015.
- Lelieveld, J., Beirle, S., Hörmann, C., Stenchikov, G., and Wagner, T.: Abrupt recent trend changes in atmospheric nitrogen dioxide over the Middle East, *Sci. Adv.*, 1, 2–6, doi:10.1126/sciadv.1500498, 2015.
- Leue, C., Wenig, M., Wagner, T., Klimm, O., Platt, U., and Jähne, B.: Quantitative analysis of NO_x emissions from Global Ozone Monitoring Experiment satellite image sequences, *J. Geophys. Res.*, 106, 5493, doi:10.1029/2000JD900572, 2001.

26591

- Levelt, P. F., Hilsenrath, E., Leppelmeier, G. W., Van Den Oord, G. H. J., Bhartia, P. K., Tamminen, J., De Haan, J. F., and Veefkind, J. P.: Science objectives of the Ozone Monitoring Instrument, *IEEE T. Geosci. Remote*, 44, 1199–1208, 2006a.
- Levelt, P. F., Van Den Oord, G. H. J., Dobber, M. R., Mälkki, A., Visser, H., De Vries, J., Stammes, P., Lundell, J. O. V., and Saari, H.: The Ozone Monitoring Instrument, *IEEE T. Geosci. Remote*, 44, 1093–1101, 2006b.
- Li, C., Marufu, L. T., Dickerson, R. R., Li, Z., Wen, T., Wang, Y., Wang, P., Chen, H., and Stehr, J. W.: In situ measurements of trace gases and aerosol optical properties at a rural site in northern China during East Asian Study of Tropospheric Aerosols: an International Regional Experiment 2005, *J. Geophys. Res.*, 112, D22S04, doi:10.1029/2006JD007592, 2007.
- Li, C., Zhang, Q., Krotkov, N. A., Streets, D. G., He, K., Tsay, S.-C., and Gleason, J. F.: Recent large reduction in sulfur dioxide emissions from Chinese power plants observed by the Ozone Monitoring Instrument, *Geophys. Res. Lett.*, 37, 1–6, doi:10.1029/2010GL042594, 2010.
- Li, C., Joiner, J., Krotkov, N. A., and Bhartia, P. K.: A fast and sensitive new satellite SO₂ retrieval algorithm based on principal component analysis: application to the ozone monitoring instrument, *Geophys. Res. Lett.*, 40, 6314–6318, doi:10.1002/2013GL058134, 2013.
- Liu, Y., Chen, X., Huang, S., Tian, L., Lu, Y., Mei, Y., Ren, M., Li, N., Liu, L., and Xiang, H.: Association between air pollutants and cardiovascular disease mortality in Wuhan, China, *Int. J. Environ. Res. Public Health*, 12, 3506–3516, doi:10.3390/ijerph120403506, 2015.
- Lookman, A. A. and Rubin, E. S.: Barriers to adopting least-cost particulate control strategies for Indian power plants, *Energy Policy*, 26, 1053–1063, doi:10.1016/S0301-4215(98)00049-4, 1998.
- Lu, Z. and Streets, D. G.: Increase in NO_x emissions from Indian thermal power plants during 1996–2010: unit-based inventories and multisatellite observations, *Environ. Sci. Technol.*, 46, 7463–7470, doi:10.1021/es300831w, 2012.
- Lu, Z., Streets, D. G., Zhang, Q., Wang, S., Carmichael, G. R., Cheng, Y. F., Wei, C., Chin, M., Diehl, T., and Tan, Q.: Sulfur dioxide emissions in China and sulfur trends in East Asia since 2000, *Atmos. Chem. Phys.*, 10, 6311–6331, doi:10.5194/acp-10-6311-2010, 2010.
- Lu, Z., Zhang, Q., and Streets, D. G.: Sulfur dioxide and primary carbonaceous aerosol emissions in China and India, 1996–2010, *Atmos. Chem. Phys.*, 11, 9839–9864, doi:10.5194/acp-11-9839-2011, 2011.

26592

- Lu, Z., Streets, D. G., De Foy, B., and Krotkov, N. A.: Ozone monitoring instrument observations of interannual increases in SO₂ emissions from Indian coal-fired power plants during 2005–2012, *Environ. Sci. Technol.*, 47, 13993–14000, doi:10.1021/es4039648, 2013.
- Lu, Z., Streets, D. G., de Foy, B., Lamsal, L. N., Duncan, B. N., and Xing, J.: Emissions of nitrogen oxides from US urban areas: estimation from Ozone Monitoring Instrument retrievals for 2005–2014, *Atmos. Chem. Phys. Discuss.*, 15, 14961–15003, doi:10.5194/acpd-15-14961-2015, 2015.
- Martin, R. V.: Satellite remote sensing of surface air quality, *Atmos. Environ.*, 42, 7823–7843, doi:10.1016/j.atmosenv.2008.07.018, 2008a.
- Martin, R. V.: Satellite remote sensing of surface air quality, *Atmos. Environ.*, 42, 7823–7843, doi:10.1016/j.atmosenv.2008.07.018, 2008b.
- Martin, R. V., Chance, K., Jacob, D. J., Kurosu, T. P., Spurr, R. J. D., Bucsela, E., Gleason, J. F., Palmer, P. I., Bey, I., Fiore, A. M., Li, Q., Yantosca, R. M., and Koelemeijer, R. B. A.: An improved retrieval of tropospheric nitrogen dioxide from GOME, *J. Geophys. Res.-Atmos.*, 107, 4437, doi:10.1029/2001JD001027, 2002.
- McLinden, C. A., Fioletov, V., Boersma, K. F., Krotkov, N., Sioris, C. E., Veefkind, J. P., and Yang, K.: Air quality over the Canadian oil sands: a first assessment using satellite observations, *Geophys. Res. Lett.*, 39, L04804, doi:10.1029/2011GL050273, 2012.
- McLinden, C. A., Fioletov, V., Boersma, K. F., Kharol, S. K., Krotkov, N., Lamsal, L., Makar, P. A., Martin, R. V., Veefkind, J. P., and Yang, K.: Improved satellite retrievals of NO₂ and SO₂ over the Canadian oil sands and comparisons with surface measurements, *Atmos. Chem. Phys.*, 14, 3637–3656, doi:10.5194/acp-14-3637-2014, 2014.
- Meibust, A. K. and Cohen, R. C.: Space-based observations of fire NO_x emission coefficients: a global biome-scale comparison, *Atmos. Chem. Phys.*, 14, 2509–2524, doi:10.5194/acp-14-2509-2014, 2014.
- MEP: The airborne pollution prevention and control action plan, available at: http://english.mep.gov.cn/News_service/infocus/201309/t20130924_260707.htm (last access: 26 August 2015), 2013.
- Mijling, B. and Van Der A, R. J.: Using daily satellite observations to estimate emissions of short-lived air pollutants on a mesoscopic scale, *J. Geophys. Res.-Atmos.*, 117, 1–20, doi:10.1029/2012JD017817, 2012.

26593

- Mijling, B., van der A, R. J., Boersma, K. F., Van Roozendaal, M., De Smedt, I., and Kelder, H. M.: Reductions of NO₂ detected from space during the 2008 Beijing Olympic Games, *Geophys. Res. Lett.*, 36, L13801, doi:10.1029/2009GL038943, 2009.
- Miyazaki, K., Eskes, H. J., and Sudo, K.: Global NO_x emission estimates derived from an assimilation of OMI tropospheric NO₂ columns, *Atmos. Chem. Phys.*, 12, 2263–2288, doi:10.5194/acp-12-2263-2012, 2012.
- Napelenok, S. L., Pinder, R. W., Gilliland, A. B., and Martin, R. V.: A method for evaluating spatially-resolved NO_x emissions using Kalman filter inversion, direct sensitivities, and space-based NO₂ observations, *Atmos. Chem. Phys.*, 8, 5603–5614, doi:10.5194/acp-8-5603-2008, 2008.
- Nowlan, C. R., Martin, R. V., Philip, S., Lamsal, L. N., Krotkov, N. A., Marais, E. A., Wang, S., and Zhang, Q.: Global dry deposition of nitrogen dioxide and sulfur dioxide inferred from space-based measurements, *Global Biogeochem. Cy.*, 28, 1025–1043, doi:10.1002/2014GB004805, 2014.
- Oetjen, H., Baidar, S., Krotkov, N. A., Lamsal, L. N., Lechner, M., and Volkamer, R.: Airborne MAX-DOAS measurements over California: testing the NASA OMI tropospheric NO₂ product, *J. Geophys. Res.-Atmos.*, 118, 7400–7413, doi:10.1002/jgrd.50550, 2013.
- Pourzamani, H., Aliyan, T., and Daryalal, M.: Evaluation of SO₂ level in the ambient air of Khark Island, *Int. J. Environ. Health Eng.*, 1, 39, doi:10.4103/2277-9183.102368, 2012.
- Reuter, M., Buchwitz, M., Hilboll, A., Richter, A., Schneising, O., Hilker, M., Heymann, J., Bovensmann, H., and Burrows, J. P.: Decreasing emissions of NO_x relative to CO₂ in East Asia inferred from satellite observations, *Nat. Geosci.*, 7, 792–795, doi:10.1038/ngeo2257, 2014.
- Richter, A. and Burrows, J. P.: Tropospheric NO₂ from GOME measurements, *Adv. Space Res.*, 2, 1–11, 2002.
- Richter, A., Burrows, J. P., Nüss, H., Granier, C., and Niemeier, U.: Increase in tropospheric nitrogen dioxide over China observed from space, *Nature*, 437, 129–132, doi:10.1038/nature04092, 2005.
- Richter, A., Begoin, M., Hilboll, A., and Burrows, J. P.: An improved NO₂ retrieval for the GOME-2 satellite instrument, *Atmos. Meas. Tech.*, 4, 1147–1159, doi:10.5194/amt-4-1147-2011, 2011.
- Richter, A., Hilboll, A., and Burrows, J. P.: Improving S5P NO₂ retrievals, available at: http://seom.esa.int/atmos2015/page_presentations.php (last access: 27 September 2015), 2015.

26594

- Rix, M., Valks, P., Hao, N., Loyola, D., Schlager, H., Huntrieser, H., Flemming, J., Koehler, U., Schumann, U., and Inness, A.: Volcanic SO₂, BrO and plume height estimations using GOME-2 satellite measurements during the eruption of Eyjafjallajökull in May 2010, *J. Geophys. Res.-Atmos.*, 117, D00U19, doi:10.1029/2011JD016718, 2012.
- 5 Russell, A. R., Valin, L. C., and Cohen, R. C.: Trends in OMI NO₂ observations over the United States: effects of emission control technology and the economic recession, *Atmos. Chem. Phys.*, 12, 12197–12209, doi:10.5194/acp-12-12197-2012, 2012.
- Schneider, P. and Van Der A, R. J.: A global single-sensor analysis of 2002–2011 tropospheric nitrogen dioxide trends observed from space, *J. Geophys. Res.-Atmos.*, 117, D16309, doi:10.1029/2012JD017571, 2012.
- 10 Schneider, P., Lahoz, W. A., and van der A, R.: Recent satellite-based trends of tropospheric nitrogen dioxide over large urban agglomerations worldwide, *Atmos. Chem. Phys.*, 15, 1205–1220, doi:10.5194/acp-15-1205-2015, 2015.
- Schoeberl, M. R., Douglass, A. R., Hilsenrath, E., Bhartia, P. K., Beer, R., Waters, J. W., Gunson, M. R., Froidevaux, L., Gille, J. C., Barnett, J. J., Levelt, P. F., and DeCola, P.: Overview of the EOS aura mission, *IEEE T. Geosci. Remote*, 44, 1066–1072, doi:10.1109/TGRS.2005.861950, 2006.
- Schumann, U. and Huntrieser, H.: The global lightning-induced nitrogen oxides source, *Atmos. Chem. Phys.*, 7, 3823–3907, doi:10.5194/acp-7-3823-2007, 2007.
- 20 Seinfeld, J. H. and Pandis, S. N.: *Atmospheric Chemistry and Physics: From Air Pollution to Climate Change*, 2nd Edn. 2006, John Wiley & Sons, Hoboken, New Jersey, 2006.
- Simon, H., Reff, A., Wells, B., Xing, J., and Frank, N.: Ozone trends across the United States over a period of decreasing NO_x and VOC emissions, *Environ. Sci. Technol.*, 49, 186–195, doi:10.1021/es504514z, 2015.
- 25 Smith, S. J., van Aardenne, J., Klimont, Z., Andres, R. J., Volke, A., and Delgado Arias, S.: Anthropogenic sulfur dioxide emissions: 1850–2005, *Atmos. Chem. Phys.*, 11, 1101–1116, doi:10.5194/acp-11-1101-2011, 2011a.
- Smith, S. J., van Aardenne, J., Klimont, Z., Andres, R. J., Volke, A., and Delgado Arias, S.: Anthropogenic sulfur dioxide emissions: 1850–2005, *Atmos. Chem. Phys.*, 11, 1101–1116, doi:10.5194/acp-11-1101-2011, 2011b.
- 30 Solomon, P. A., Crumpler, D., Flanagan, J. B., Jayanty, R. K. M., Rickman, E. E., and McDade, C. E.: US national PM_{2.5} Chemical Speciation Monitoring Networks-CSN and IM-

26595

- PROVE: description of networks, *J. Air Waste Manage.*, 64, 1410–1438, available at: <http://www.ncbi.nlm.nih.gov/pubmed/25562937> (last access: 7 August 2015), 2014.
- Stavrakou, T., Müller, J.-F., Boersma, K. F., De Smedt, I., and van der A, R. J.: Assessing the distribution and growth rates of NO_x emission sources by inverting a 10-year record of NO₂ satellite columns, *Geophys. Res. Lett.*, 35, L10801, doi:10.1029/2008GL033521, 2008.
- 5 Streets, D. G., Canty, T., Carmichael, G. R., de Foy, B., Dickerson, R. R., Duncan, B. N., Edwards, D. P., Haynes, J. A., Henze, D. K., Houyoux, M. R., Jacob, D. J., Krotkov, N. A., Lamsal, L. N., Liu, Y., Lu, Z., Martin, R. V., Pfister, G. G., Pinder, R. W., Salawitch, R. J., and Wecht, K. J.: Emissions estimation from satellite retrievals: a review of current capability, *Atmos. Environ.*, 77, 1011–1042, doi:10.1016/j.atmosenv.2013.05.051, 2013.
- 10 Theys, N., De Smedt, I., van Gent, J., Danckaert, T., Wang, T., Hendrick, F., Stavrakou, T., Bauduin, S., Clarisse, L., Li, C., Krotkov, N., Yu, H., Brenot, H., and Van Roozendael, M.: Sulfur dioxide vertical column DOAS retrievals from the Ozone Monitoring Instrument: global observations and comparison to ground-based and satellite data, *J. Geophys. Res.-Atmos.*, 120, 2470–2491, doi:10.1002/2014JD022657, 2015.
- 15 Tian, H., Qiu, P., Cheng, K., Gao, J., Lu, L., Liu, K., and Liu, X.: Current status and future trends of SO₂ and NO_x pollution during the 12th FYP period in Guiyang city of China, *Atmos. Environ.*, 69, 273–280, doi:10.1016/j.atmosenv.2012.12.033, 2013.
- Tong, D. Q., Lamsal, L., Pan, L., Ding, C., Kim, H., Lee, P., Chai, T., Pickering, K. E., and Stajner, I.: Long-term NO_x trends over large cities in the United States during the great recession: comparison of satellite retrievals, ground observations, and emission inventories, *Atmos. Environ.*, 107, 70–84, doi:10.1016/j.atmosenv.2015.01.035, 2015.
- 20 Twohy, C. H.: Nitrogenated organic aerosols as cloud condensation nuclei, *Geophys. Res. Lett.*, 32, L19805, doi:10.1029/2005GL023605, 2005.
- 25 US Department of Veterans Affairs: Sulfur Fire at Mishraq State Sulfur Mine – Public Health, available at: <http://www.publichealth.va.gov/exposures/mishraq-sulfur-fire/index.asp> (last access: 25 August 2015), 2015.
- US EIA: Coal plants without scrubbers account for a majority of US SO₂ emissions – today in energy, U.S. Energy Information Administration (EIA), available at: <http://www.eia.gov/todayinenergy/detail.cfm?id=4410> (last access: 9 August 2015), 2010.
- 30 US EPA: National Emissions Inventory (NEI) Air Pollutant Emissions Trends Data, available at: <http://www.epa.gov/ttnchie1/trends/> (last access: 7 August 2015), 2014.

26596

- US EPA: Six Common Air Pollutants, Air and Radiation, US EPA, available at: <http://www3.epa.gov/ttn/chieftrends/> (last access: 27 September 2015), 2015.
- Valin, L. C., Russell, A. R., and Cohen, R. C.: Variations of OH radical in an urban plume inferred from NO₂ column measurements, *Geophys. Res. Lett.*, 40, 1856–1860, doi:10.1002/grl.50267, 2013.
- Valks, P., Pinardi, G., Richter, A., Lambert, J.-C., Hao, N., Loyola, D., Van Roozendael, M., and Emmadi, S.: Operational total and tropospheric NO₂ column retrieval for GOME-2, *Atmos. Meas. Tech.*, 4, 1491–1514, doi:10.5194/amt-4-1491-2011, 2011.
- Van der A, R. J., Peters, D. H. M. U., Eskes, H., Boersma, K. F., Van Roozendael, M., De Smedt, I., and Kelder, H. M.: Detection of the trend and seasonal variation in tropospheric NO₂ over China, *J. Geophys. Res.-Atmos.*, 111, 1–10, doi:10.1029/2005JD006594, 2006.
- Van der A, R. J., Eskes, H. J., Boersma, K. F., van Noije, T. P. C., Van Roozendael, M., De Smedt, I., Peters, D. H. M. U., and Meijer, E. W.: Trends, seasonal variability and dominant NO_x source derived from a ten year record of NO₂ measured from space, *J. Geophys. Res.*, 113, D04302, doi:10.1029/2007JD009021, 2008.
- Vautard, R., Cattiaux, J., Yiou, P., Thépaut, J.-N., and Ciais, P.: Northern Hemisphere atmospheric stilling partly attributed to an increase in surface roughness, *Nat. Geosci.*, 3, 756–761, doi:10.1038/ngeo979, 2010.
- Veefkind, J. P., Aben, I., McMullan, K., Förster, H., de Vries, J., Otter, G., Claas, J., Eskes, H. J., de Haan, J. F., Kleipool, Q., van Weele, M., Hasekamp, O., Hoogeveen, R., Landgraf, J., Snel, R., Tol, P., Ingmann, P., Voors, R., Kruizinga, B., Vink, R., Visser, H., and Levelt, P. F.: TROPOMI on the ESA Sentinel-5 Precursor: a GMES mission for global observations of the atmospheric composition for climate, air quality and ozone layer applications, *Remote Sens. Environ.*, 120, 70–83, doi:10.1016/j.rse.2011.09.027, 2012.
- Vestreng, V., Ntziachristos, L., Semb, A., Reis, S., Isaksen, I. S. A., and Tarrasón, L.: Evolution of NO_x emissions in Europe with focus on road transport control measures, *Atmos. Chem. Phys.*, 9, 1503–1520, doi:10.5194/acp-9-1503-2009, 2009.
- Vinken, G. C. M., Boersma, K. F., van Donkelaar, A., and Zhang, L.: Constraints on ship NO_x emissions in Europe using GEOS-Chem and OMI satellite NO₂ observations, *Atmos. Chem. Phys.*, 14, 1353–1369, doi:10.5194/acp-14-1353-2014, 2014a.
- Vinken, G. C. M., Boersma, K. F., Maasakkers, J. D., Adon, M., and Martin, R. V.: Worldwide biogenic soil NO_x emissions inferred from OMI NO₂ observations, *Atmos. Chem. Phys.*, 14, 10363–10381, doi:10.5194/acp-14-10363-2014, 2014b.

26597

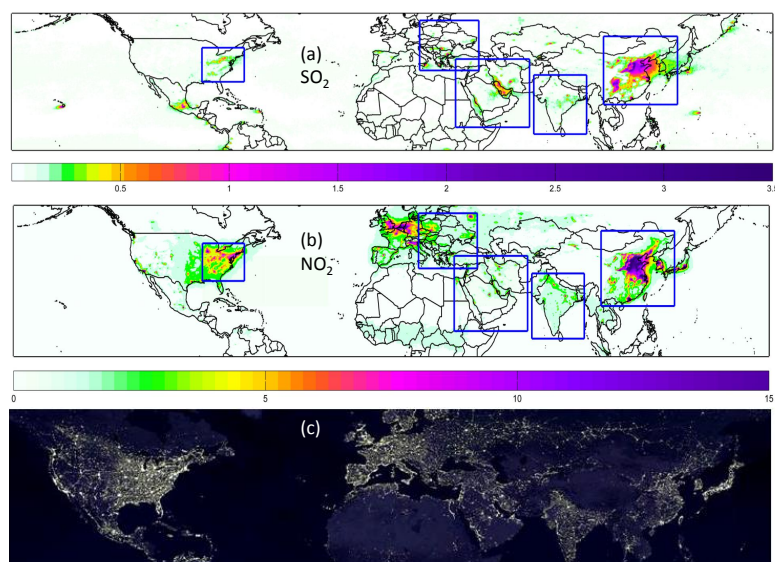
- Witte, J. C., Schoeberl, M. R., Douglass, A. R., Gleason, J. F., Krotkov, N. A., Gille, J. C., Pickering, K. E., and Livesey, N.: Satellite observations of changes in air quality during the 2008 Beijing Olympics and Paralympics, *Geophys. Res. Lett.*, 36, L17803, doi:10.1029/2009GL039236, 2009.
- Zhang, Q., Streets, D. G., He, K., Wang, Y., Richter, A., Burrows, J. P., Uno, I., Jang, C. J., Chen, D., Yao, Z., and Lei, Y.: NO_x emission trends for China, 1995–2004: the view from the ground and the view from space, *J. Geophys. Res.-Atmos.*, 112, D22306, doi:10.1029/2007JD008684, 2007.
- Zhang, Q., Streets, D. G., and He, K.: Satellite observations of recent power plant construction in Inner Mongolia, China, *Geophys. Res. Lett.*, 36, L15809, doi:10.1029/2009GL038984, 2009.
- Zhang, X.-P. and Cheng, X.-M.: Energy consumption, carbon emissions, and economic growth in China, *Ecol. Econ.*, 68, 2706–2712, doi:10.1016/j.ecolecon.2009.05.011, 2009.
- Zhao, B., Wang, S., Wang, J., Fu, J. S., Liu, T., Xu, J., Fu, X., and Hao, J.: Impact of national NO_x and SO₂ control policies on particulate matter pollution in China, *Atmos. Environ.*, 77, 453–463, doi:10.1016/j.atmosenv.2013.05.012, 2013.
- Zhou, Y., Brunner, D., Boersma, K. F., Dirksen, R., and Wang, P.: An improved tropospheric NO₂ retrieval for OMI observations in the vicinity of mountainous terrain, *Atmos. Meas. Tech.*, 2, 401–416, doi:10.5194/amt-2-401-2009, 2009.
- Zhou, Y., Brunner, D., Hueglin, C., Henne, S., and Staehelin, J.: Changes in OMI tropospheric NO₂ columns over Europe from 2004 to 2009 and the influence of meteorological variability, *Atmos. Environ.*, 46, 482–495, doi:10.1016/j.atmosenv.2011.09.024, 2012.
- Zyrichidou, I., Koukoulis, M. E., Balis, D. S., Katragkou, E., Poupkou, A., Kioutsioukis, I., Markakis, K., Melas, D., Van Der A, R., Boersma, F. K., and Van Roozendael, M.: Comparison of satellite NO₂ observations with high resolution model simulations over the Balkan Peninsula, in: AIP Conference Proceedings, Vol. 1203, 632–637, 2010.
- Zyrichidou, I., Koukoulis, M. E., Balis, D. S., Kioutsioukis, I., Poupkou, A., Katragkou, E., Melas, D., Boersma, K. F., and van Roozendael, M.: Evaluation of high resolution simulated and OMI retrieved tropospheric NO₂ column densities over southeastern Europe, *Atmos. Res.*, 122, 55–66, doi:10.1016/j.atmosres.2012.10.028, 2013.

26598

Table A1. Filtering transient volcanic clouds.

Region	Threshold (DU)	Days excluded (2005–2014)
Eastern US	5	97
Eastern Europe	8	72
Eastern China	10	71
India	8	58
Middle East	8	10

26599

**Figure 1.** OMI-derived maps of PBL SO₂ in Dobson Units [DU] **(a)** and tropospheric NO₂ columns in [10¹⁵ molecules cm⁻²] **(b)** for 2005–2007 show enhanced pollution levels around major cities and industrial centers, seen also in the “Earth at Night” (city lights) map **(c)**, courtesy of Aura EPO team.

26600

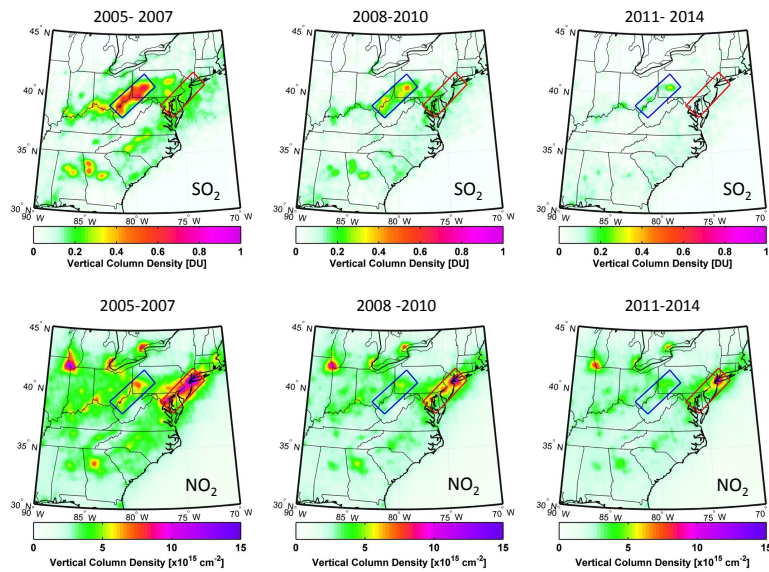


Figure 2. Multiyear average OMI SO₂ (top) and tropospheric NO₂ (bottom) regional maps over eastern US for 3 periods: 2005–2007, 2008–2010 and 2011–2014. Blue box outlines Ohio River Valley and SW Pennsylvania (ORV) region with largest SO₂ emissions from coal-fired power plants. Red box outlines megalopolis from Washington, DC to New York along the I-95 interstate highway (I-95 corridor) with largest NO₂ from mobile sources.

26601

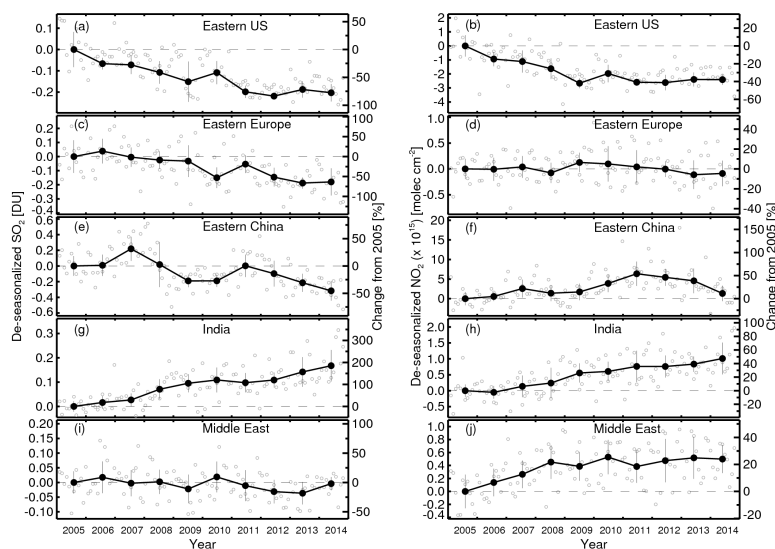


Figure 3. Relative changes (compared to 2005) in OMI PBL SO₂ columns (left) and tropospheric NO₂ columns (right) over 5 world's most polluted regions: **(a and b)**: Ohio River Valley and western Pennsylvania (ORV) in eastern US (ORV – blue box in Fig. 2); **(c and d)**: Maritsa Iztok Power Plants in Bulgaria (blue box in Fig. 4); **(e and f)**: North China Plane (NCP – blue box in Fig. 5); **(g and h)**: NE India (blue box in Fig. 6); **(i and j)**: Persian Gulf (blue box in Fig. 7). Gray circles show de-seasonalized monthly columns (see details in Supplement). Black filled circles show annual means. Vertical bars show standard deviations.

26602

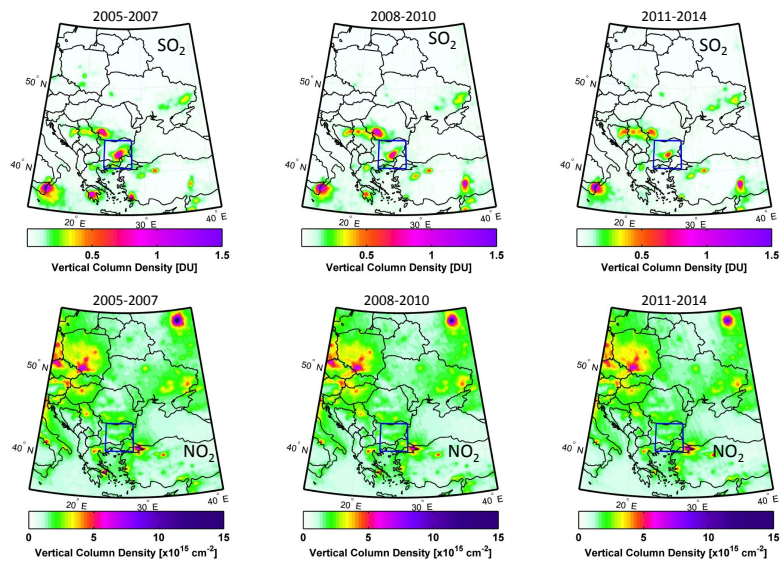


Figure 4. Same as Fig. 2, but for Eastern Europe. The largest SO₂ source in the domain is the Etna volcano in Sicily, Italy. The blue box is centered on SO₂ polluted area around Maritsa Iztok coal mining region and the largest coal-fired power plant in southeastern Bulgaria.

26603

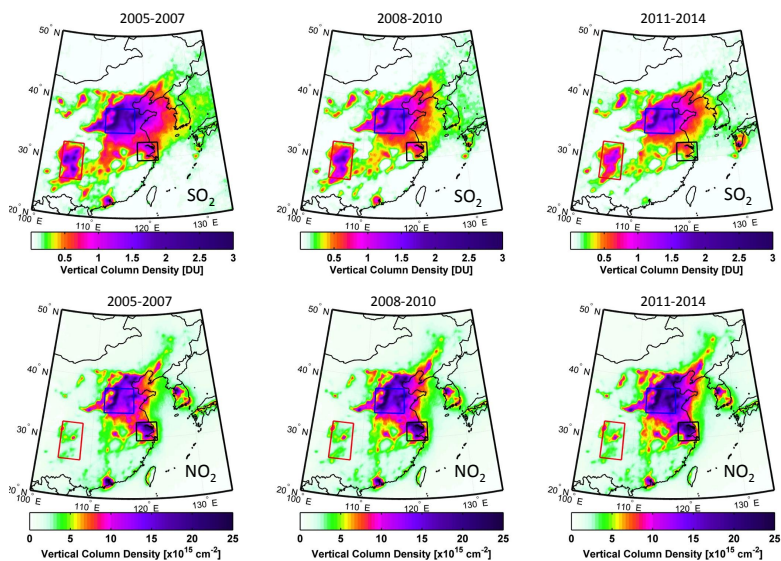


Figure 5. Similar to Fig. 2 but for eastern China. Blue box outlines North China Plane (NCP) also represented in Fig. 3, red box – Sichuan Basin (SB) and black box represent Yangtze River Delta (YRD). The boxes are also shown in Figs. S1, S3 and S4.

26604

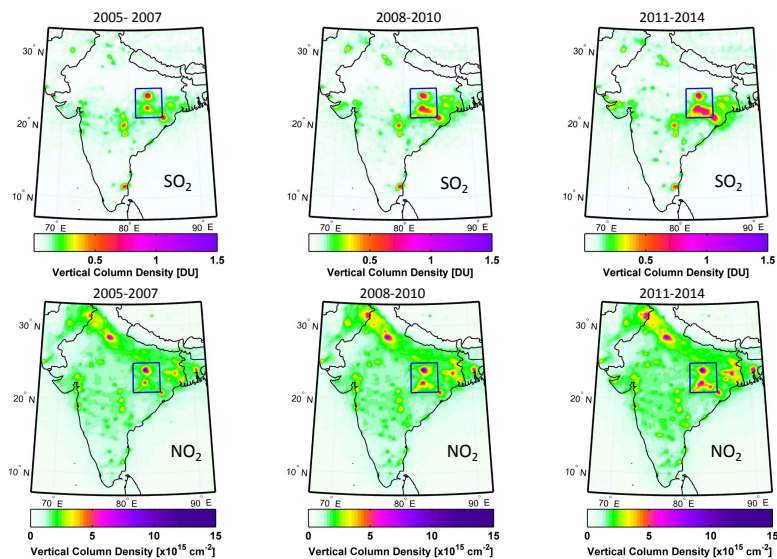


Figure 6. Similar to Fig. 2 but for India. Blue box outlines industrial regions in Chhattisgarh and Odisha, one of India's most active areas in terms of building new coal-fired power plants. The region is shown in Fig. 3.

26605

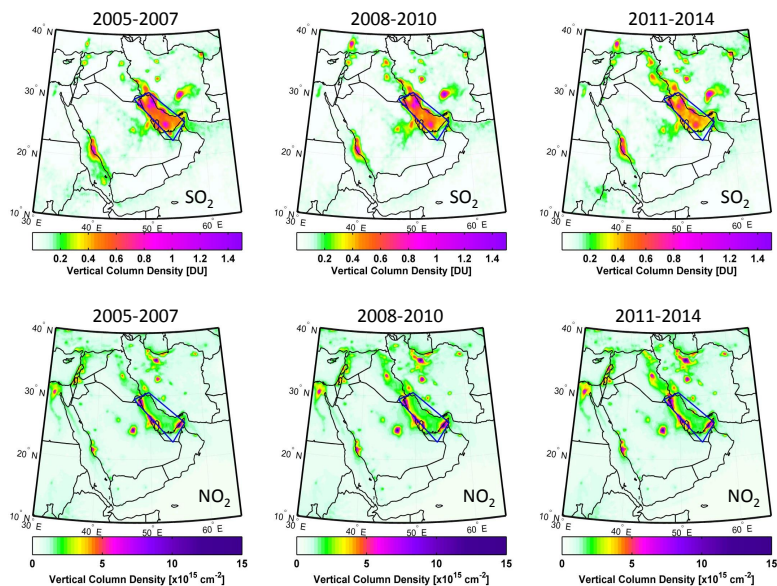


Figure 7. Similar to Fig. 2 but for the Middle East. Blue box outlines Persian Gulf region with high SO₂ and NO₂ levels due to oil and gas operations.

26606

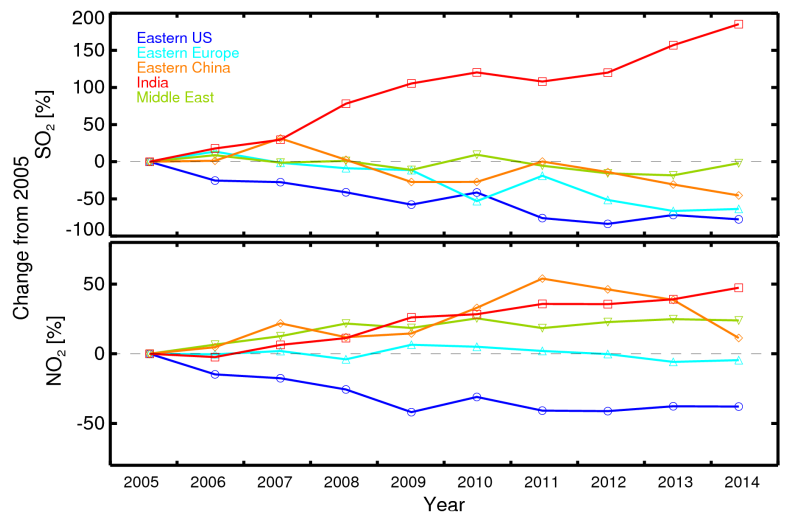


Figure 8. Percent change in OMI annual average columns: SO₂ (top) and NO₂ (bottom) over the world's most polluted regions.